Research Square

Preprints are preliminary reports that have not undergone peer review.
They should not be considered conclusive, used to inform clinical practice,
or referenced by the media as validated information.

Reversible m6Am methylation of snRNA by FTO controls morphine reward and tolerance without altering analgesia

Ying-Xian Pan

yx.pan@rutgers.edu

Rutgers New Jersey Medical School https://orcid.org/0000-0002-4006-8304

Shan Liu

Rutgers New Jersey Medical School

Ayma Malik

Rutgers New Jersey Medical School

Raymond Chien

Rutgers New Jersey Medical School https://orcid.org/0009-0005-1731-2312

Jianheng Liu

Weill Cornell Medicine, Cornell University https://orcid.org/0000-0003-0216-1951

Luke Nicholson

Weill Cornell Medical College https://orcid.org/0009-0005-8203-7249

Jin Xu

Rutgers New Jersey Medical School

Kimia Didehvar

Rutgers New Jersey Medical School

Vipin Rai

Rutgers New Jersey Medical School

Valerie Le Rouzic

Memorial Sloan-Kettering Cancer Center

Arlene Martínez-Rivera

Temple University

Konstantinos Boulias

Washington University School of Medicine

Bing Wang

Rutgers New Jersey Medical School

Anjali Rajadhyaksha

Temple University https://orcid.org/0000-0002-8399-5466

Yuan-Xiang Tao

Rutgers New Jersey Medical School https://orcid.org/0000-0003-1777-3272

Eric Greer

Washington University School of Medicine in St. Louis https://orcid.org/0000-0002-7501-7371

Samie Jaffrey

Weill Cornell Medicine, Cornell University https://orcid.org/0000-0003-3615-6958

Article

Keywords:

Posted Date: November 2nd, 2026

DOI: https://doi.org/10.21203/rs.3.rs-10747158/v1

License: This work is licensed under a Creative Commons Attribution 4.0 International License.
Read Full License

Additional Declarations: Yes there is potential Competing Interest. S.R.J. is the co-founder and/or has equity in Chimerna Therapeutics, 858 Therapeutics, and Lucerna Technologies. Y.-X.P. is a scientific co-founder of Sparian Biosciences. Rutgers University has filed US Nonprovisional Patent Application 19/756,799, “Pharmaceutical formulations and methods” (inventor: Y.-X.P)

Reversible m^{6}Am methylation of snRNA by FTO controls morphine reward and tolerance without altering analgesia

Shan Liu[1,2,9], Ayma F. Malik[1,2,9], Raymond Chien[1,2,9], Jianheng Liu[3,9], Luke S. Nicholson[3,9], Jin Xu[1,2,4], Kimia Didehvar[1,2], Vipin Rai[1,2], Valerie P. Le Rouzic[4], Arlene Martínez-Rivera[5,6,7], Konstantinos Boulias[8], Bing Wang[1], Anjali M. Rajadhyaksha[5,6,7], Yuan-Xian Tao[1], Eric Lieberman Greer[8], Samie R. Jaffrey[3,✉], Ying-Xian Pan[1,2,4,✉]

[1]Department of Anesthesiology, New Jersey Medical School, Newark, NJ 07103, USA. [2]Rutgers Addiction Research Center, Brain Health Institute, Rutgers Health, Piscataway, NJ 08854, USA. [3]Department of Pharmacology, Weill Cornell Medical College, Cornell University, New York, NY 10065, USA. [4]Department of Neurology, Memorial Sloan-Kettering Cancer Center, New York, NY, 10065, USA. [5]Division of Pediatric Neurology, Department of Pediatrics, Weill Cornell Medicine, New York, NY 10065, USA. [6]Center for Substance Abuse Research and Department of Neural Sciences, Lewis Katz School of Medicine at Temple University, Philadelphia, PA 19140, USA. [7]Feil Family Brain and Mind Research Institute, Weill Cornell Medicine, New York, NY 10065, USA. [8]Department of Pediatrics, Washington University School of Medicine, St. Louis, MO, 63110, USA. [9] These authors contributed equally: Shan Liu, Ayma F. Malik, Raymond Chien, Jianheng Liu, Luke S. Nicholson. ✉e-mail: srj2003@med.cornell.edu. ✉e-mail: yx.pan@rutgers.edu

Abstract

Mu opioids, such as morphine, are effective analgesics, but they produce reward and tolerance that lead to opioid use disorder. A major goal is to achieve analgesia without these harmful effects. Here we show that morphine reward and tolerance are controlled by a reversible RNA modification in small nuclear RNA (snRNA) that is removed by the RNA demethylase FTO. Genetic depletion and pharmacologic inhibition of FTO each reduced morphine reward, measured by conditioned-place preference, and reduced tolerance to morphine and fentanyl, without altering analgesia. Depleting *Fto* in the nucleus accumbens shell reduced reward but not tolerance, while depleting *Fto* in the dorsal root ganglion reduced tolerance but not reward, suggesting region-specific effects of FTO. Although FTO is known to erase m^6A on mRNA, we found no effect of FTO depletion on m^6A sites, but a marked increase in m^6Am levels in snRNA. The effects of FTO depletion were suppressed in mice that cannot make m^6Am, supporting the importance of elevated m^6Am in suppressing morphine reward and tolerance. Consistent with altered snRNA function, FTO depletion reshapes gene expression linked to morphine signaling. FTO inhibitors may therefore provide useful adjuvants for mu opioids in pain management and treatment of opioid use disorder.

Mu opioids, including natural derivatives like morphine and synthetic analogs such as fentanyl, remain the standard for managing moderate to severe pain in clinical settings, despite associated side effects like tolerance, reward and addiction. However, the misuse or illegal use of these mu opioids often leads to opioid use disorder, a primary driver of the global opioid epidemic and rising rates of overdose deaths[1-4]. A major goal is to develop pain treatment strategies in which the analgesic effects of morphine are retained while the risk of opioid use disorder is minimized.

Mu opioids produce analgesia, tolerance, and reward through the mu opioid receptors (MORs). These effects diverge downstream of MORs, at the level of signaling pathways, cell types, and circuits. Reward and addiction depend on the nucleus accumbens (NAc), ventral tegmental area (VTA), and prefrontal cortex (mPFC)[5-9]. Tolerance has been linked to N-methyl-D-aspartate (NMDA) receptors[10], nitric oxide signaling[11,12], P-glycoprotein[13], cAMP signaling[14,15], alternatively spliced *Oprm1*[16], MOR/DOR heterodimerization[17,18], protein kinase C (PKC) pathways[19,20], β-arrestin signaling[21,22], PDGFβ[23], and MOR trafficking[24]. It remains challenging to target these pathways to block tolerance and reward while preserving analgesia.

Fat mass and obesity-associated protein (FTO), also known as alpha-ketoglutarate-dependent dioxygenase, is an RNA demethylase that has been shown to affect diverse neuronal signaling mechanisms[25-28]. FTO is abundantly expressed in both the central and peripheral nervous systems[29-31] and can influence gene expression by modulating mRNA stability, alternative splicing, translation, and epigenetic regulation[27,28,32-35]. More significantly, FTO has been implicated in various neuronal functions, including locomotion[36], stress response[37], and the sensation of neuropathic pain[31], as well as in several neuropsychiatric disorders such as Alzheimer's disease, Parkinson's disease, epilepsy, anxiety, and depression[38-40].

Early studies showed that the mechanism of FTO involves demethylating N^6-methyladenosine (m^6A)[25,26], a modified nucleotide enriched in mRNA. The effects of FTO have primarily been linked to demethylation of m^6A in specific transcripts[41]. FTO has been reported to target specific mRNAs, maintaining m^6A sites in these transcripts at low levels. Upon FTO depletion, m^6A levels rise, thus causing mRNA instability or other effects on these mRNAs[41]. More recent studies have shown that FTO can also demethylate N^6,2'-O-dimethyladenosine (m^6Am) with a catalytic efficiency of up to 100 times greater than that for m^6A[27,28]. m^6Am is located at the first transcribed nucleotide in both mRNA and small nuclear RNA (snRNA), but FTO primarily demethylates m^6Am in snRNA, leading to the formation of 2'-O-methyladenosine in snRNA. By regulating these epitranscriptomic pathways, FTO can influence diverse neuronal functions.

Here we assessed the role of FTO in the analgesic, reward, and tolerance effects of morphine. Using either genomic deletion of *Fto* or pharmacologic inhibition of FTO we found that FTO is required to establish morphine reward and antinociceptive tolerance of morphine. However, depleting FTO does not alter morphine analgesia. We found that depleting *Fto* in the nucleus accumbens shell (NAcSh) reduced reward but not tolerance, while depleting *Fto* in the dorsal root ganglion (DRG) reduced tolerance but not reward. To determine how FTO produces these effects, we mapped m^6A in control and FTO-depleted NAcSh transcriptome. We saw no change in m^6A stoichiometry across 20,139 detected m^6A sites. Instead, we found that FTO depletion led to a marked increase in m^6Am in snRNA, as well as altered gene expression patterns in genes linked to morphine signaling pathway. To determine whether the effects of FTO depletion were due to increased m^6Am levels, we examined the effects of FTO depletion in mice lacking m^6Am due to depletion of PCIF1, the enzyme that synthesizes m^6Am. In these mice,

92 m^6Am levels cannot increase, and FTO depletion was no longer able to suppress morphine
93 reward and tolerance. Overall, these data point to m^6Am levels in snRNA as a key regulator of
94 morphine reward and tolerance and suggest that FTO inhibitors may be useful adjuvants to mu
95 opioid in pain management and opioid use disorder treatment.
96
97 **Targeting FTO reduces morphine-induced conditioned place preference**
98 To investigate the role of FTO in opioid reward, we assessed the acquisition of morphine
99 conditioned place preference (CPP) in *Fto*$^{+/-}$ mice using a 6-day CPP paradigm (**Fig. 1a**). *Fto*
100 homozygous knockout (KO) mice were excluded from these studies owing to their increased
101 postnatal mortality and developmental delays[42]. *Fto*$^{+/-}$ mice exhibited a significant reduction in
102 morphine CPP scores relative to wild-type C57BL/6 (WT-B6) mice (**Fig. 1b**), indicating that
103 partial loss of *Fto* is sufficient to impair the acquisition of morphine CPP. Morphine analgesia
104 assessed using the hot plate assay was unaffected in *Fto*$^{+/-}$ mice (**Fig. 1c**), demonstrating that
105 reducing *Fto* selectively modulates the rewarding properties of morphine without altering its
106 antinociceptive potency and efficacy.

107 To extend these findings pharmacologically, we examined the effect of the selective,
108 potent FTO inhibitor FB23-2[43] on morphine CPP acquisition in both *Fto*$^{fl/fl}$ and WT-B6 mice.
109 Vehicle (DMSO) or 20 μg of FB23-2 was intracerebroventricularly (i.c.v.) administered, two
110 hours prior to each morphine conditioning session over four consecutive days (Days 2–5) (**Fig.**
111 **1d**). FB23-2 significantly attenuated the acquisition of morphine CPP in both *Fto*$^{fl/fl}$ and WT-B6
112 mice (**Figs. 1e, 1f**). FB23-2 administered alone, in the absence of morphine, produced no CPP
113 (**Figs. 1i, 1j**), confirming that the observed attenuation reflects suppression of morphine's
114 rewarding properties rather than a non-specific effect on CPP behavior.

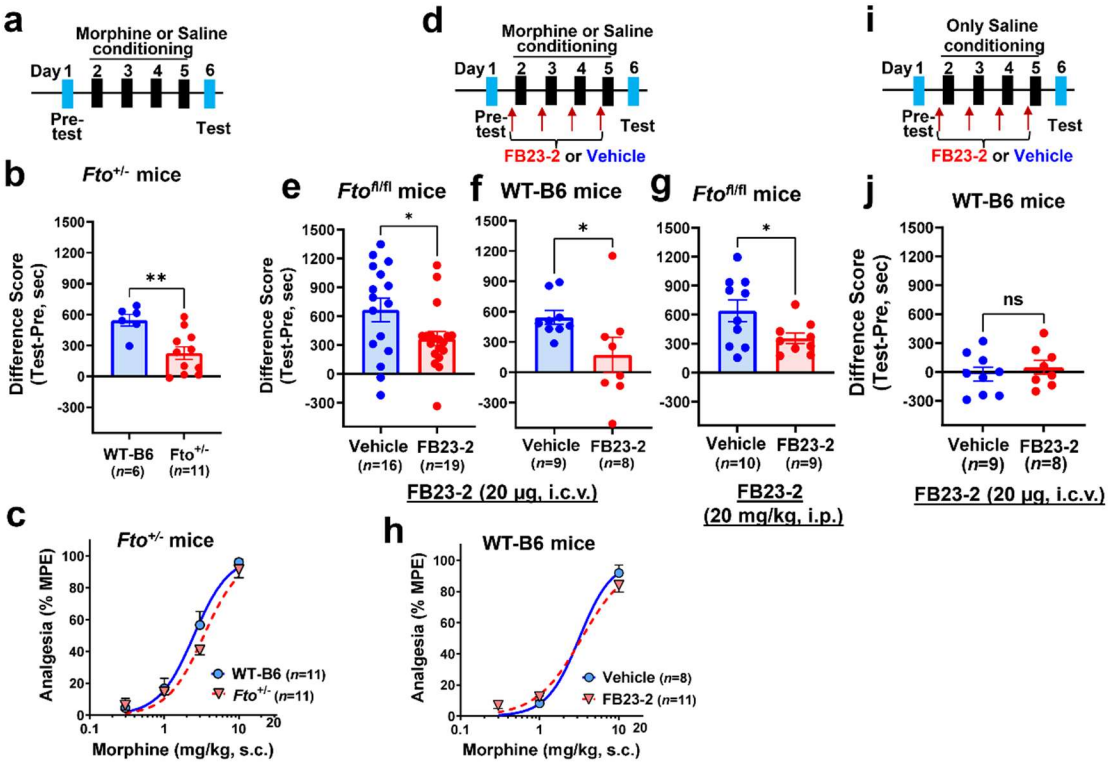


Fig. 1. **Targeting FTO reduced morphine reward. a.** Schematic of morphine CPP in male Fto heterozygous (*Fto*$^{+/-}$) mice. **b**. Reduced morphine CPP in *Fto*$^{+/-}$ mice. Preference (Difference Score) was calculated as described in Methods. **: $p < 0.01$, two-tailed Student *t*-test. **c.** No change of morphine analgesia in *Fto*$^{+/-}$ mice. Morphine analgesic dose-response was measured using a Hot-plate assay and quantified as the percentage of maximum possible effect (% MPE) as described in the Methods. The ED_{50} values were calculated using non-linear regression analysis (GraphPad Prism 10). The ED_{50} in WT-B6 mice, 2.48 mg/kg, 95% confident intervals (CIs), 1.78 – 3.46. The ED_{50} in *Fto*$^{+/-}$ mice, 3.38 mg/kg, 95% CIs, 2.70 – 4.24. There was no significant difference in the ED_{50} values between WT-B6 and *Fto*$^{+/-}$ mice, as determined by an extra sum-of-square F-test ($p = 0.1230$). **d.** Schematic of morphine CPP in mice treated with FB23-2 for E, F & G. **e, f.** Reduced morphine CPP by i.c.v. administration of FB23-2 in *Fto*$^{fl/fl}$ **(e)** or WT-B6 mice **(f)**. FB23-2 (20µg) or Vehicle (DMSO) was i.c.v. administered 2 hours before morphine conditioning for 4 consecutive days (Day 2 – Day 5). *: $p < 0.05$, two-tailed Student *t*-test. **g**. Reduced morphine CPP by i.p. administration of FB23-2 in *Fto*$^{fl/fl}$ mice. 20 mg/kg of FB23-2 or DMSO was i.p. administered 2 hours before morphine conditioning for 4 consecutive days (Day 2 – Day 5). *: $p < 0.05$, two-tailed Student *t*-test. **h.** No change of morphine analgesia in WT-B6 mice. Morphine analgesic dose-response was measured using a Hot-plate assay and quantified as in c. The ED_{50} values were calculated as in c. The ED_{50} in WT-B6 mice treated i.c.v. FB23-2, 3.45 mg/kg, 95% confident intervals (CIs), 2.58 – 4.61. The ED_{50} in WT-B6 mice treated i.c.v. Vehicle, 3.38 mg/kg, 95% confident intervals (CIs), 2.07 – 5.52. There was no significant difference in the ED_{50} values between WT-B6 mice treated with FB23-2 and Vehicle, as determined by the extra sum-of-square F-test ($p = 0.9249$). **i.** Schematic of CPP in WT-B6 mice treated with i.c.v. FB23-2 or Vehicle. 20µg of FB23-2 or Vehicle (DMSO) was i.c.v. administered 2 hours before second saline conditioning. **j.** No effect of FB23-2 on saline CPP in WT-B6 mice. n.s.: No statistical significance, two-tailed Student *t*-test.

We next assessed morphine analgesia following i.c.v. administration of FB23-2. Morphine analgesia, evaluated using the hot plate assay, was similarly unaffected (**Fig. 1h**), reinforcing the

idea that pharmacological inhibition of FTO selectively attenuates the acquisition of morphine CPP without compromising its analgesia potency and efficacy.

Since FB23-2 has been reported to penetrate the blood-brain barrier following systemic administration[44], we next asked whether intraperitoneal (i.p.) delivery would recapitulate the suppression of morphine CPP acquisition observed with i.c.v. administration, thereby establishing a more tractable route of inhibition. *Fto*$^{fl/fl}$ mice received FB23-2 (20 mg/kg, i.p.) two hours prior to morphine conditioning over four consecutive days (Days 2–5). Consistent with the i.c.v. findings, systemic FB23-2 administration significantly attenuated the acquisition of morphine CPP (**Fig. 1g**), demonstrating that peripheral delivery of an FTO inhibitor is sufficient to suppress morphine CPP, further supporting the feasibility of targeting FTO pharmacologically to mitigate morphine reward.

Selective depletion of FTO in the NAcSh reduces morphine reward

Having established that both genetic reduction and pharmacological inhibition of FTO attenuate the acquisition of morphine CPP, we next sought to identify the brain region through which FTO acts to modulate morphine reward. The nucleus accumbens shell (NAcSh) is a key node of the mesolimbic reward circuitry and has been directly implicated in the rewarding properties of opioids[45-47].

To test whether FTO within the NAcSh is required for morphine CPP, *Fto* was selectively depleted in this region by bilateral stereotaxic microinjection of adenovirus expressing Cre recombinase/GFP under the control of the cytomegalovirus (CMV) promoter (AAV5-CMV-Cre/GFP; hereafter AAV-Cre) into *Fto*$^{fl/fl}$ mice, with AAV5-CMV-GFP (AAV-GFP) serving as the control. The viral transduction and efficiency of FTO depletion were examined by GFP imaging

combined with RNAScope *in situ* hybridization using *Fto*-specific probes in the same brain sections. GFP imaging revealed robust expression of Cre/GFP and GFP transduced by AAV-Cre or AAV-GFP, respectively, in the NAcSh (**Fig. 2a**), confirming transduction by both AAV vectors. RNAScope in situ hybridization showed that over 95% of *Fto* transcripts were eliminated in the NAcSh of AAV-Cre-injected mice, with no detectable effect on *Fto* mRNA levels in AAV-GFP-injected controls (**Fig. 2a**).

We assessed morphine CPP in mice five weeks after viral transduction. Mice underwent morphine CPP acquisition using the 6-day paradigm described above (**Fig. 2b**). $Fto^{fl/fl}$ mice receiving NAcSh microinjections of AAV-Cre exhibited significantly lower morphine CPP scores than AAV-GFP-injected controls (**Fig. 2c**). Taken together, these results demonstrate that selective depletion of *Fto* within the NAcSh is sufficient to impair the acquisition of morphine-induced CPP, identifying the NAcSh as a key locus through which FTO regulates morphine reward.

FTO inhibitors markedly reduce morphine antinociceptive tolerance

Having demonstrated that FTO modulates morphine reward, we next asked whether FTO also governs the development of morphine antinociceptive tolerance. Antinociceptive tolerance was induced in WT-B6 mice by subcutaneous (s.c.) administration of morphine (10 mg/kg, twice daily) over five days, a well-established protocol for producing robust antinociceptive tolerance[16]. FB23-2 (20 mg/kg, i.p.) or vehicle (DMSO) was administered two hours prior to the first morphine injection each day throughout the five-day period. Analgesia was assessed using

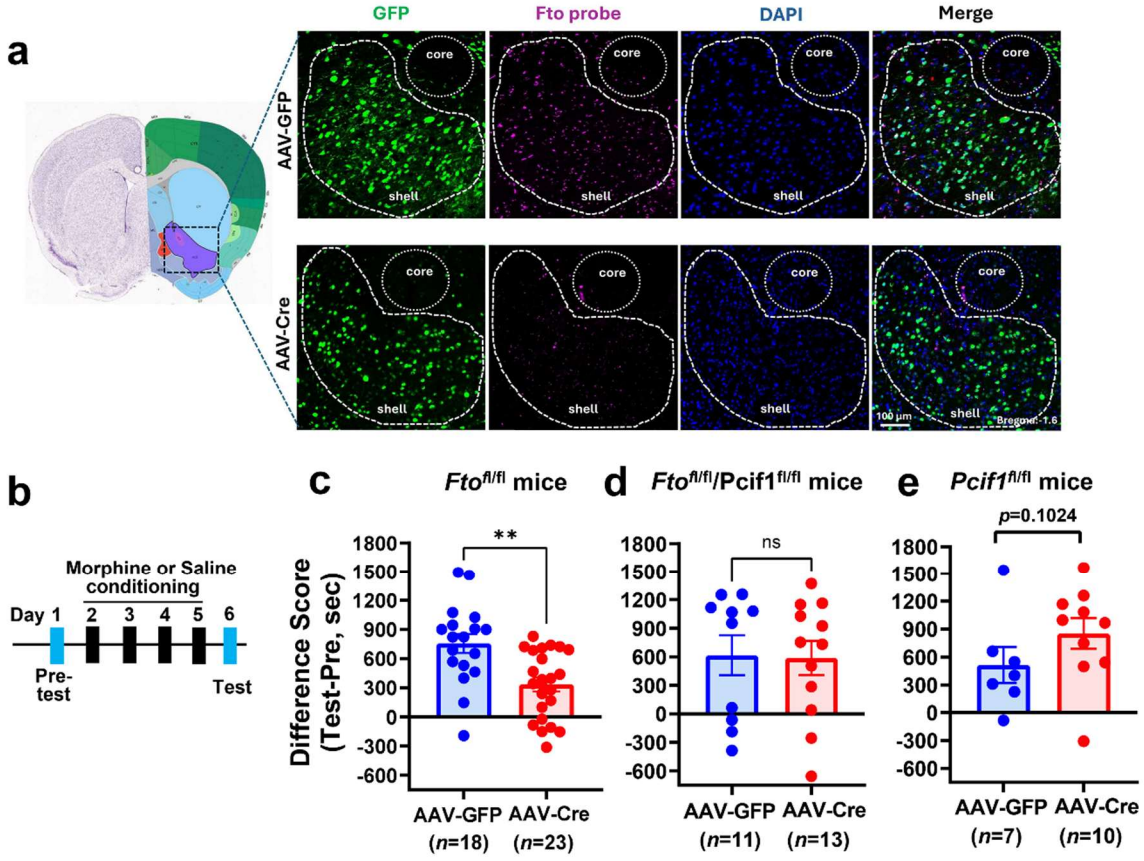


Fig 2. Targeting FTO in the NAcSh reduced morphine reward. a. Depletion of Fto in the NAcSh using microinjected AAV-Cre/GFP. RNAscope with Fto probe and Fto/GFP imaging was performed on brain sections from *Fto*$^{fl/fl}$ mice microinjected with AAV-Cre/GFP or AAV-GFP in the NAcSh after morphine CPP study, as described in the Methods. AAV-Cre: AAV5-CMV-Cre/GFP; AAV-GFP: AAV5-CMV-GFP; core: NAc core; shell: NAc shell (NAcSh). **b.** Schematic of CPP. **c.** Reduced morphine CPP by disrupting Fto in the NAcSh via AAV-Cre in *Fto*$^{fl/fl}$ mice. *Fto*$^{fl/fl}$ mice were bilaterally microinjected in the NAcSh with AAV-Cre/GFP or AAV-GFP. Morphine CPP was performed as in Fig. 1a five weeks post-injection. **: $p < 0.01$, two-tailed Student *t*-test. **d.** No significant changes in morphine CPP by disrupting both Fto and Pcif1 in the NAcSh in *Fto*$^{fl/fl}$;*Pcif1*$^{fl/fl}$ mice. *Fto*$^{fl/fl}$;*Pcif1*$^{fl/fl}$ mice were microinjected in the NAcSh with AAV-Cre/GFP or AAV-GFP. Morphine CPP was performed as in Fig. 2b five weeks post-injection. n.s.: No statistical significance, two-tailed Student *t*-test. **e.** No significant changes in morphine CPP by disrupting Pcif1 in the NAcSh in *Pcif1*$^{fl/fl}$ mice. *Pcif1*$^{fl/fl}$ mice were microinjected in the NAcSh with AAV-Cre/GFP or AAV-GFP. Morphine CPP was performed as shown in Fig. 2b five weeks post-injection. $p = 0.1024$, no statistical significance, two-tailed Student *t*-test.

the radiant heat tail-flick assay through morphine dose-response curves on Days 1 and 5 and following the second morphine dose (10 mg/kg) on Days 3 and 4. Morphine antinociceptive tolerance was readily apparent in vehicle-treated mice by Days 4 and 5 (**Fig. 3a**). In contrast, FB23-2-treated mice exhibited significantly attenuated morphine antinociceptive tolerance, as

reflected in the time course (**Fig. 3a**) and dose-response curves, which had a smaller rightward shift in ED_{50} between Days 1 and 5 relative to vehicle-treated controls (**Fig. 3b** & **Table 1**).

We next examined the effect of FB23-2 on morphine tolerance in WT B6 mice through intrathecal (i.t.) administration. 20 μg of FB23-2 or vehicle (DMSO) was administered i.t. two hours prior to the first morphine injection each day for five days. Similar to i.p. administration, Intrathecal FB23-2 significantly attenuated the development of antinociceptive tolerance on Days 4 and 5, as reflected in the time course (**Fig. 3c**) and dose-response curves with a much smaller rightward shift in ED_{50} between Days 1 and 5 relative to vehicle-treated controls (**Fig. 3d** & **Table 1**).

To confirm that the effect of FB23-2 on morphine antinociceptive tolerance is not background-dependent, we conducted an identical morphine tolerance study in WT B6-like *Fto*$^{fl/fl}$ mice. Systemic FB23-2 (20 mg/kg, i.p.) similarly attenuated morphine antinociceptive tolerance on Days 4 and 5 in these mice (**Fig. 3e**), with a minimal rightward shift in ED_{50} between Days 1 and 5 relative to vehicle-treated controls (**Fig. 3f** & **Table 1**), consistent with the findings in WT-B6 mice.

Fentanyl is a commonly used opioid analgesics in clinic and displays distinct pharmacological profiles that set it apart from opium-derived morphine[48]. We next asked whether FTO inhibition extends to fentanyl antinociceptive tolerance. Fentanyl antinociceptive tolerance was induced by continuous s.c. delivery via an osmotic pump (Alzet Model 1007D; 1 mg/kg/day for 7 days). Analgesia was assessed using the radiant heat tail-flick assay through fentanyl dose-response curves on Days 1 and 7 and following a single fentanyl challenge (0.12 mg/kg) on Days 3, 5, and 6. FB23-2 (20 mg/kg, i.p.) or vehicle was co-administered once daily throughout the 7-day period. FB23-2 significantly attenuated the development of fentanyl antinociceptive

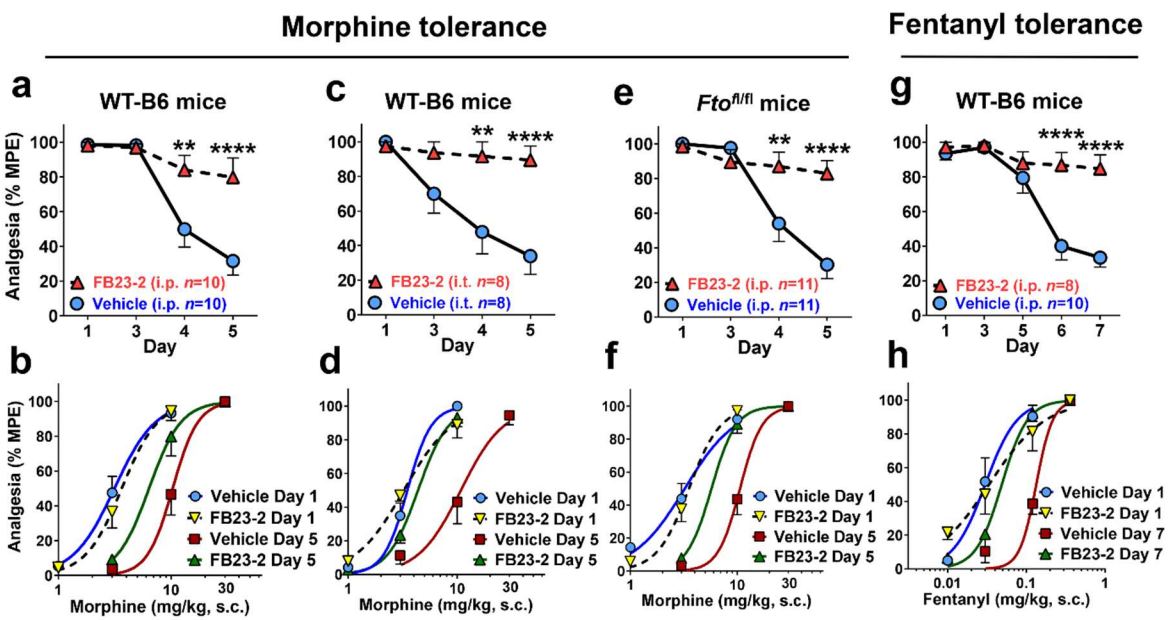


Fig. 3. Targeting FTO reduced mu opioid nociceptive tolerance. a, b. Reduced morphine tolerance by i.p. administration of FB23-2 in WT-B6 mice. FB23-2 (20 mg/kg) and DMSO (vehicle) were i.p. administered daily 2 hours before the first morphine dosing for 5 days in WT-B6 mice. **a**: Time course; **b**: Dose-response curve. **c, d.** Reduced morphine tolerance by i.t. administration of FB23-2 in WT-B6 mice. FB23-2 (20 μg) and DMSO (vehicle) were i.t. administered daily 2 hours before the first morphine dose for 5 days in WT-B6. **c**: Time course; **d**: Dose-response curve. **e, f.** Reduced morphine tolerance by i.p. administration of FB23-2 in *Fto*$^{fl/fl}$ mice. FB23-2 (20 mg/kg) and DMSO (vehicle) were i.p. administered daily 2 hours before the first morphine dose for 5 days in *Fto*$^{fl/fl}$ mice. **e**: Time course; **f**: Dose-response curve. **g, h.** Reduced fentanyl tolerance by i.p. administration of FB23-2 in WT-B6 mice. FB23-2 (20 mg/kg) and DMSO (vehicle) were i.p. administered daily for 7 days in WT-B6 mice. Fentanyl tolerance was induced by an s.c. implanted osmotic pump (Alzet Model: 1007D; 1 mg/kg/day/mouse for 7 days). **g**: Time course; **h**: Dose-response curve. Morphine or fentanyl analgesia was measured by using a radiant heat tail-flick assay and quantified as the percentage of maximum possible effect (% MPE) as described in the Methods. All ED_{50} values were calculated using non-linear regression analysis (GraphPad Prism 10) and listed on Table 1. **: $p < 0.01$; ****: $p < 0.0001$, 2-way ANOVA with Bonferroni's *post hoc* test.

tolerance on Days 6 and 7, as reflected in the time course (**Fig. 3g**) and dose-response curves, with a reduced rightward shift in ED_{50} between Days 1 and 7 relative to vehicle-treated controls (**Fig. 3h** & **Table 1**).

Taken together, these findings demonstrate that FTO is required for the development of antinociceptive tolerance to both morphine and fentanyl, and that pharmacological inhibition of

Table 1. Mu opioid analgesic dose-responses in tolerance studies

Mouse model	Drug or AAV	Route	# of mice	Morphine ED_{50} (mg/kg, s.c.)[A]		ED_{50} shift
				Day 1	Day 5	
WT-B6	FB23-2	i.p.	10	3.7 (2.9-4.5)	6.4 (4.9-8.3)[B,C]	1.7
	Vehicle	i.p.	10	3.2 (2.6-3.8)	10.3 (8.8-12.1)[B]	3.3
WT-B6	FB23-2	i.t.	8	3.2 (2.7-3.9)	4.4 (3.6-5.4)[C]	1.3
	Vehicle	i.t.	8	3.5 (2.9-4.3)	10.8 (8.0-14.6)[B]	3.1
Fto$^{fl/fl}$	FB23-2	i.p.	11	3.5 (3.0-4.1)	5.7 (4.8-6.9)[B,C]	1.6
	Vehicle	i.p.	11	3.2 (2.5-4.2)	10.6 (9.1-12.4)[B]	3.3
Fto$^{fl/fl}$	NAcSh-Cre		10	3.6 (2.7-4.7)	10.8 (9.0-12.9)	3.0
	NAcSh-GFP		9	4.1 (3.7-7.0)	10.9 (8.5-14.9)	2.7
Fto$^{fl/fl}$;AvCreERT2	Tamoxifen	i.p.	12	3.8 (2.9-4.5)	5.1 (4.1-5.5)	1.3
	Vehicle	i.p.	14	3.5 (2.7-4.4)	10.6 (8.4-13.3)	3.0
Fto$^{fl/fl}$;*Pcif1*$^{fl/fl}$;AvCreERT2	Tamoxifen	i.p.	8	4.3 (3.5-6.2)	11.6 (9.3-14.3)	2.7
	Vehicle	i.p.	6	3.4 (1.9-4.9)	10.6 (8.8-12.5)	3.1
				Fentanyl ED_{50} (µg/kg, s.c.)[A]		ED_{50} shift
				Day 1	Day 7	
WT-B6	FB23-2	i.p.	8	33.6 (22-51)	48.0 (36-66)[C]	1.5
	Vehicle	i.p.	10	30.1 (22-42)	133.9 (109-164)[B]	4.0

[A]: ED50 values with 95% confidence intervals (Cis) were determined by nonlinear regression analysis (Prism). ED_{50} values with nonoverlapping 95% Cis were considered significantly different[16]. [B]: $p<0.05$, compared with Day 1; [C]: $p<0.05$, compared with Vehicle.

235

236 FTO with FB23-2 markedly attenuates this process across multiple routes of administration and

237 mu opioid compounds.

238

Targeting FTO in the DRG attenuates morphine antinociceptive tolerance

The DRG has been established as a critical site for the involvement of opioid antinociceptive tolerance[49-63]. Having shown that systemic and intrathecal FTO inhibition attenuates the development of morphine antinociceptive tolerance, we next sought to determine whether *Fto* expression in DRG sensory neurons specifically accounts for this effect. To achieve inducible, DRG-restricted *Fto* depletion, we used *Fto*$^{fl/fl}$;AvCreERT2 mice, generated by crossing *Fto*$^{fl/fl}$ mice with Advillin-CreERT2 (AvCreERT2) mice in which CreERT2 expression is driven by the Advillin promoter and is therefore restricted to DRG sensory neurons[64]. Following i.p. administration of tamoxifen (75 mg/kg) for 10 consecutive days, *Fto* transcript levels were markedly depleted in the DRG (**Fig. 4a**). Morphine antinociceptive tolerance was then assessed using the 5-day paradigm described above. Tamoxifen-treated *Fto*$^{fl/fl}$;AvCreERT2 mice exhibited markedly attenuated morphine antinociceptive tolerance relative to vehicle-treated controls (**Figs 4b, c**), demonstrating that *Fto* expression in DRG sensory neurons is required for the full development of morphine antinociceptive tolerance. On the other hand, Fto depletion by tamoxifen in *Fto*$^{fl/fl}$;AvCreERT2 mice had no effect on morphine CPP (**Fig. 4d**), demonstrating that *Fto* in the DRG selectively modulates morphine tolerance without impacting its rewarding properties.

The NAc also involves morphine tolerance in addition to morphine reward[65-68]. The results above, combined with the previous NAcSh-specific depletion data, raised the question of whether the NAcSh, the primary locus governing FTO-dependent morphine reward, also contributes to morphine antinociceptive tolerance. To address this directly, morphine antinociceptive tolerance was assessed in *Fto*$^{fl/fl}$ mice following bilateral NAcSh microinjection of AAV-Cre or AAV-GFP. *Fto*$^{fl/fl}$ mice receiving NAcSh injections of AAV-Cre exhibited a

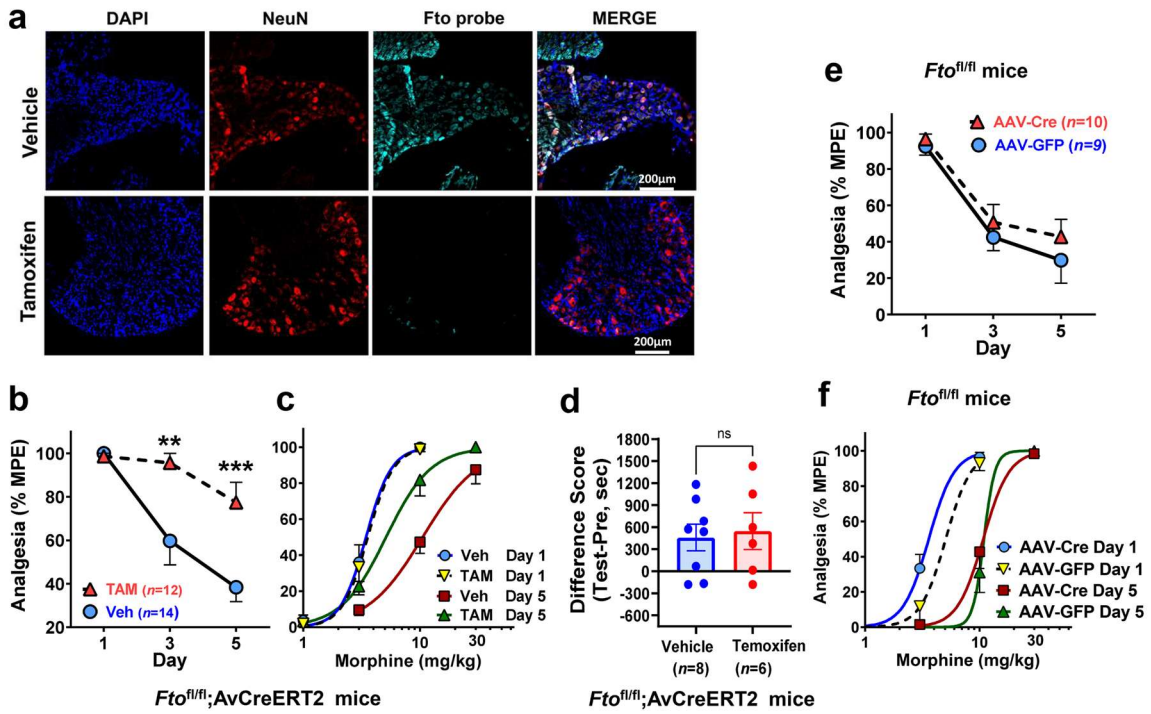


Fig. 4. Targeting FTO in the DRG reduced morphine nociceptive tolerance. a. Depletion of Fto in the DRG sensory neurons using tamoxifen in *Fto*$^{fl/fl}$;AvCreERT2 mice. Tamoxifen (75 mg/kg) or Corn oil (Vehicle) was i.p. administered daily in *Fto*$^{fl/fl}$;AvCreERT2 mice for 10 days. RNAScope combined with IHC with anti-NeuN antibody was performed on the DRG sections from perfused mice (4% PFA) after morphine tolerance study, as described in the Methods. **b, c.** Depleting Fto in the DRG sensory neurons attenuated morphine tolerance in *Fto*$^{fl/fl}$;AvCreERT2 mice. Morphine analgesia was measured by using a radiant heat tail-flick assay and quantified as described in the Methods. The ED_{50} values were calculated using non-linear regression analysis (GraphPad Prism 10) and listed on Table 1. **b**: Time course; **c**: Dose-response curve. **: $p < 0.01$; ***: $p < 0.001$, 2-way ANOVA with Bonferroni's *post hoc* test. **d.** Depleting Fto in the DRG sensory neurons had no effect on morphine CPP in *Fto*$^{fl/fl}$;AvCreERT2 mice. Morphine CPP was performed same as Fig. 1a. n.s: no statistical significance, two-tailed Student *t*-test. **e, f.** Depleting Fto in the NAcSh had no significant effect on morphine tolerance in *Fto*$^{fl/fl}$ mice. Morphine tolerance in *Fto*$^{fl/fl}$ mice microinjected with AAV-Cre or AAV-GFP was performed same as **b** (**e**, time course) & **c** (**f**, dose-response curve). No statistical significance, 2-way ANOVA with Bonferroni's *post hoc* test.

morphine tolerance profile indistinguishable from that of AAV-GFP-injected controls, both in terms of the time course and the rightward shift in ED_{50} between Days 1 and 5 (**Figs 4e, f**). These findings indicate that *Fto* within the NAcSh does not contribute to morphine antinociceptive tolerance. Instead, FTO in the DRG contributes to the development of morphine antinociceptive tolerance.

FTO depletion selectively increases snRNA m^{6}Am levels in the NAcSh transcriptome

Our finding that FTO depletion in the NAcSh impairs morphine-induced CPP suggests that RNA modification levels markedly influence the rewarding properties of morphine. The canonical substrate of FTO is m^6A, which FTO demethylates in specific transcripts, thereby maintaining those mRNAs in a hypomethylated state[41]. Loss of FTO is therefore expected to result in elevated m^6A stoichiometry at regulated sites, with downstream consequences including enhanced mRNA decay through m^6A-dependent degradation pathways. To determine whether this mechanism accounts for the effects of FTO depletion on morphine reward, we mapped m^6A sites across the NAc transcriptome using Oxford Nanopore direct RNA sequencing of poly(A)+ RNA[69-76]. NAc tissue was harvested five weeks after bilateral microinjection of AAV-GFP or AAV-Cre into *Fto*$^{fl/fl}$ mice. Four biological replicates of each condition were sequenced, and m^6A stoichiometry values showed high concordance across replicates at sites covered by a minimum of 25 independent reads per replicate (**Extended Data Figs. 1a, b, Supplementary Data Table 1**). To maximize the number of sites meeting this coverage threshold, reads from the four replicates were merged for each condition, yielding ~990,000 primary-mapped reads. m^6A stoichiometry was then compared between conditions at all sites with a minimum coverage of 25 independent reads and a minimum stoichiometry of 0.05.

Comparison of m^6A stoichiometries in AAV-GFP and AAV-Cre revealed a high similarity in m^6A stoichiometry across all detected sites between FTO-depleted and control NAcSh samples. This contrasts with FTO studies in leukemia where specific m^6A sites in the *MYC* mRNA show marked increases in m6A levels after FTO depletion[77]. This indicates that FTO depletion produces no specific m^6A sites that have clear increases in m^6A levels in the NAcSh transcriptome (**Figs. 5a**, **b**).

Since m^{6}A stoichiometry was unaffected by FTO depletion, we next examined whether FTO instead regulates levels of m^{6}Am, the other established FTO substrate. m^{6}Am occupies the first transcribed nucleotide position in both mRNAs and snRNAs. To analyze m^{6}Am, we previously developed CROWN-seq to specifically capture and quantify the stoichiometry at the first nucleotide[78]. In CROWN-seq, unmethylated 2'-*O*-methyladenosine (Am) is chemically deaminated into 2'-*O*-methylinosine (Im), which appears in sequencing data as G. However, m^{6}Am resists deamination and therefore appears as A. Thus, the percent of transcripts that contain A at the first transcribed position indicates the stoichiometry of m^{6}Am.

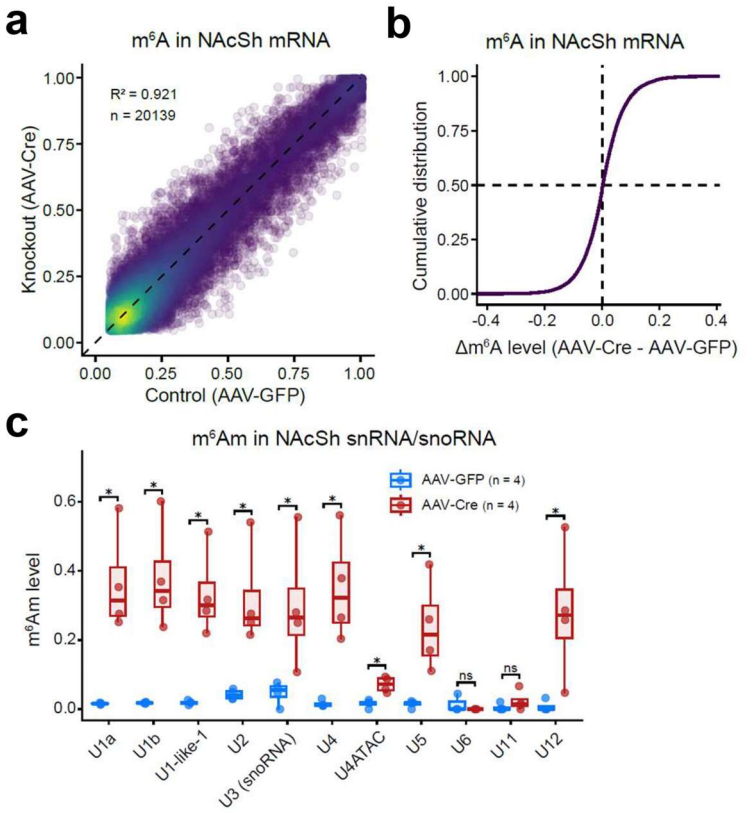


Fig. 5. m^{6}A and m^{6}Am profiling in the *Fto*$^{fl/fl}$ NAcSh upon FTO depletion. a. Scatter plot comparing site-specific m^{6}A stoichiometries between AAV-Cre and AAV-GFP treated *Fto*$^{fl/fl}$ mice NAcSh tissue (n = 20,139 shared sites, ⩾25 reads). Each condition consists of four biological replicates merged for stoichiometry calculation. Pearson's coefficient of determination is given by $R^2 = 0.921$. **b.** Cumulative distribution plot of m^{6}A differences between AAV-Cre and AAV-GFP treated samples (Δm^{6}A = Cre – GFP). **c.** Boxplots of m^{6}Am stoichiometry in different snRNA and snoRNA transcripts. For each condition, four biological replicates were shown. Compared with AAV-GFP control NAcSh, AAV-Cre NAcSh show a robust increase in m^{6}Am at most snRNA and snoRNA (U3). Only transcripts with ⩾25 read coverage for each replicate are shown. Statistical significance determined by a Wilcoxon rank-sum test for each snRNA/snoRNA type (ns, non-significant, *$p < 0.05$).

CROWN-seq analysis revealed that m^6Am levels in snRNA were markedly elevated in FTO-depleted NAcSh relative to controls (**Fig. 5c, Extended Data Fig. 1c**, **Supplementary Data Table 2**). Analysis at the level of individual snRNA species revealed particularly prominent increases in m^6Am in U1, U2, U4, U5, and U12 snRNA, along with the U3 snoRNA, with mean m^6Am stoichiometries rising from a range of 0.008-0.042 under control conditions to 0.240-0.381 following FTO depletion (**Fig. 5c**, **Supplementary Data Table 2**) . The maximum increase for any given replicate was found to be +0.580 for the U1b snRNA. Notably, this data demonstrates that FTO in the NAcSh very efficiently demethylates m^6Am in snRNAs to near-zero levels in basal conditions, and that, upon conditional knockout of FTO, these levels can rise substantially.

Taken together, these data demonstrate that FTO depletion in the NAcSh does not alter m^6A stoichiometry at any detectable site in the transcriptome but instead produces widespread increases in m^6Am levels in snRNAs, most prominently in U1. These findings suggest that the mechanism of FTO inhibition does not involve the canonical m^6A pathway but instead points to the less explored m^6Am-snRNA axis as the molecular basis for FTO's role in morphine reward.

Targeting *Pcif1* abolishes the effect of FTO depletion on morphine reward

To determine whether the increase in m^6Am upon FTO depletion is causally required for the suppression of morphine reward, we employed a genetic epistasis strategy using $Fto^{fl/fl}$;$Pcif1^{fl/fl}$ mice. PCIF1 is the methyltransferase responsible for m^6Am synthesis; accordingly, *Pcif1* depletion abolishes m^6Am and prevents any FTO depletion-dependent increase in this modification. If FTO depletion mediates its effects on morphine reward by elevating m^6Am,

FTO depletion should no longer have an effect in *Fto*$^{fl/fl}$;*Pcif1*$^{fl/fl}$ mice when m6Am synthesis is blocked by *Pcif1* deletion.

To test this prediction, both *Fto* and *Pcif1* were simultaneously depleted in the NAcSh of *Fto*$^{fl/fl}$;*Pcif1*$^{fl/fl}$ mice by bilateral AAV-Cre microinjection, with AAV-GFP serving as the control. Successful elimination of both *Fto* and *Pcif1* transcripts was confirmed by RNAScope in situ hybridization in AAV-Cre-injected mice relative to AAV-GFP-injected controls (**Extended Data Fig. 2**). Five weeks after injection, mice underwent morphine CPP acquisition using the 6-day paradigm described above. In AAV-GFP-injected *Fto*$^{fl/fl}$;*Pcif1*$^{fl/fl}$ mice, morphine induced robust CPP (**Fig. 2d**). However, in contrast to *Fto* depletion alone which impaired morphine-induced CPP, depletion of *Fto* along with *Pcif1* restored morphine-induced CPP acquisition (**Fig. 2d**). These results demonstrate that the suppression of morphine CPP by FTO depletion requires the capacity to elevate m^{6}Am, establishing increased m^{6}Am in snRNA as the causal mediator of FTO's effect on morphine reward.

Since increased m^{6}Am caused by FTO depletion reduces morphine-induced CPP, we next asked if reduced m^{6}Am would enhance the acquisition of morphine-induced CPP. Although m^{6}Am is already low in snRNA (see **Fig. 5c**), we nevertheless measured morphine CPP acquisition in *Pcif1*$^{fl/fl}$ mice following NAcSh microinjection of AAV-Cre or AAV-GFP. NAcSh-specific depletion of *Pcif1* led to increased CPP scores compared to the AAV-GFP group, but this did not achieve statistical significance ($p = 0.1024$) (**Fig. 2e**). Nevertheless, the trend toward increased CPP scores raises the possibility that endogenous m^{6}Am levels in the NAcSh are inversely correlated with morphine reward as measured by CPP.

Targeting *Pcif1* abolishes the effect of FTO depletion on morphine antinociceptive tolerance

Having established that elevated m^6Am in snRNA mediates the suppression of morphine reward by FTO depletion in the NAcSh, we next asked whether the same mechanism accounts for the attenuation of morphine antinociceptive tolerance produced by FTO depletion in the DRG. To test this, a parallel genetic epistasis approach was employed in $Fto^{fl/fl}$;$Pcif1^{fl/fl}$;Advillin-CreERT2 mice, enabling inducible, DRG-restricted co-depletion of both *Fto* and *Pcif1* by tamoxifen administration. Successful elimination of both *Fto* and *Pcif1* transcripts in the DRG was confirmed by RNAScope in situ hybridization in tamoxifen-treated mice relative to vehicle-treated controls (**Extended Data Fig. 3**).

Morphine antinociceptive tolerance was then assessed using the 5-day paradigm described above. Vehicle-treated controls developed robust morphine antinociceptive tolerance, as expected. In contrast to *Fto* depletion, co-depletion of both *Fto* and *Pcif1* in the DRG was associated with restored morphine antinociceptive tolerance. Morphine antinociceptive tolerance in *Fto* and *Pcif1* depleted mice achieved levels comparable to those of vehicle-treated controls (**Figs. 6a, b**). These results demonstrate that the attenuation of morphine antinociceptive tolerance produced by DRG-specific FTO depletion is mediated through its capacity to elevate m^6Am, establishing increased m^6Am as a causal determinant of both morphine reward and antinociceptive tolerance.

Impact of FTO depletion on alternative splicing

We next asked how increased m^6Am could affect gene expression related to morphine reward and tolerance. Our data, as well as previous studies[27], show that FTO primarily regulates m^6Am

on snRNA, not mRNA. However, the function of the m^6Am form of snRNA compared to the more abundant Am form of snRNA is not known. The canonical function of snRNAs is in pre-mRNA splicing, where they direct intron recognition and removal as core components of the spliceosome[79]. However, U1 snRNA serves an additional, splicing-independent function to suppress premature cleavage and polyadenylation at cryptic intronic sites, thereby sustaining transcriptional elongation through intronic regions and ensuring production of full-length transcripts[80,81]. Elevated m^6Am in U1 snRNA and other snRNA species following FTO depletion could therefore perturb either spliceosome fidelity and telescripting activity, with broad consequences for gene expression in the NAcSh.

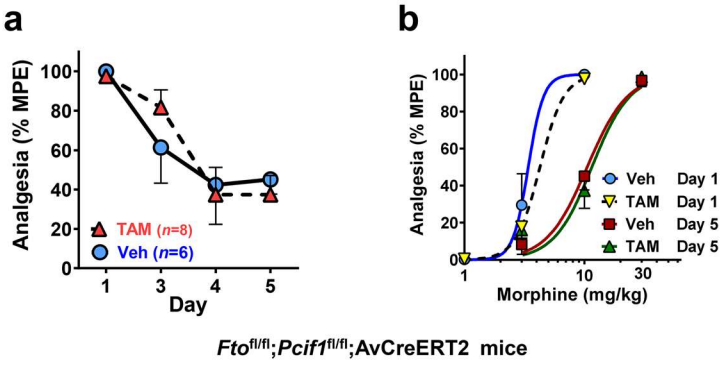


Fig. 6. Depletion of FTO along with PCIF1 in the DRG restores morphine nociceptive tolerance. a, b. Morphine tolerance was performed in *Fto*$^{fl/fl}$;*Pcif1*$^{fl/fl}$;AvCreERT2 mice after treatment of tamoxifen or vehicle same as Figs. 4b, 4c. The ED_{50} values were calculated using non-linear regression analysis (GraphPad Prism 10) and listed on Table 1. **a**: Time course; **b**: Dose-response curve.

To distinguish transcriptomic changes strictly attributable to FTO depletion from those induced by opioid exposure, we performed RNA-seq on NAc tissue harvested from *Fto*$^{fl/fl}$ mice that received bilateral AAV-GFP or AAV-Cre microinjections and underwent the CPP paradigm without morphine exposure.

We first examined the impact of Fto depletion on splicing. We performed alternative splicing analysis with rMATS[82] (**Extended Data Fig. 4, Supplementary Data Table 3**). The major splicing change in Fto-depleted NAc is exon skipping, although other types of alternative splicing were also found (**Fig. 7a**). In total, we observed 552 significant exon skipping events

across 483 genes (FDR <0.1), as well as other forms of alternative splicing. Alternative splicing was seen across diverse types of genes, without a clear enrichment in specific Gene Ontology pathways (**Supplementary Data Table 3**).

We next asked whether FTO depletion affects U1 snRNA-dependent transcriptional elongation. U1 snRNA promotes elongation through introns and 3'UTRs, which preferentially enhances expression of long genes[80]. We performed differential gene expression analysis between control and FTO-depleted NAcSh. We found 2,176 upregulated genes and 1,901 downregulated genes (adjusted $p < 0.1$) (**Fig. 7b, Supplementary Data Table 4**). The upregulated genes had significantly longer gene bodies than the downregulated and unchanged genes (median 37.6 kbp versus 23.5 and 23.2 kbp) (**Fig. 7c**). This length bias indicates that elevated m^6Am promotes U1-dependent elongation of long genes. FTO depletion raises snRNA m^6Am, so FTO normally opposes this elongation and limits expression of long genes.

Impact of FTO depletion on genes in morphine addiction pathways

We next asked whether the transcriptomic changes produced by FTO depletion converge on genes that control morphine reward. We performed Gene Set Enrichment Analysis (GSEA) of the differentially expressed genes against KEGG pathways. Many signaling pathways were altered, and the morphine addiction pathway was significantly enriched among the genes changed in the FTO-depleted NAcSh (**Fig. 7d**, **Supplementary Data Table 5**).

Many of these genes were altered in a coordinated direction that opposes MOR-driven reward signaling in the GABAergic interneuron/D1-MSN circuit of the NAc shell, the circuit through which morphine produces reward[45,83,84] (**Figs. 7e, f**). MOR normally suppresses presynaptic

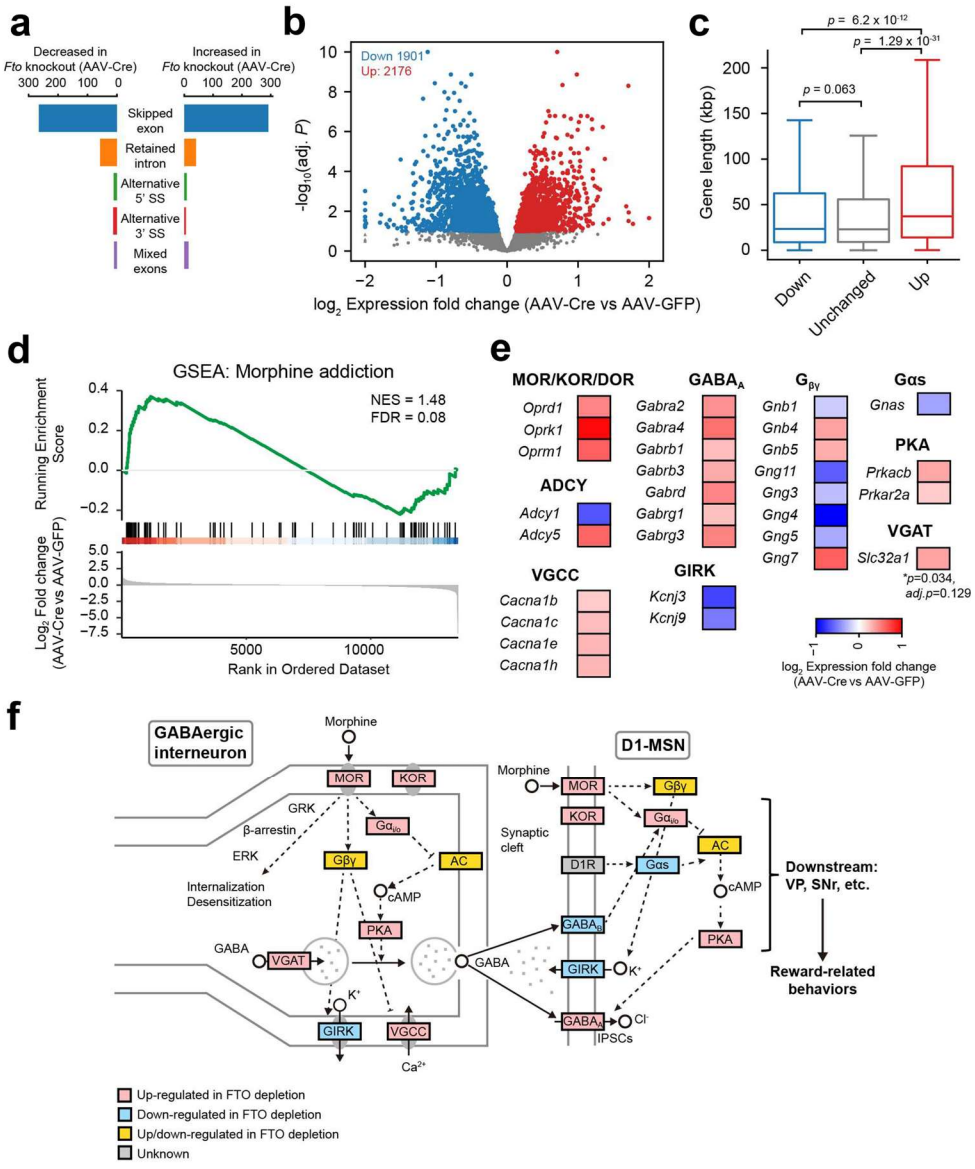


Fig. 7. The transcriptomic changes in *Fto*$^{fl/fl}$ NAcSh upon FTO depletion. a. The number of alternative splicing events found between AAV-Cre (Fto knockout) and AAV-GFP (control). The corresponding volcano plots can be found in **Extended Data Fig. 4**. **b.** A volcano plot showing genes with significant differential expression upon FTO depletion. Genes with at least 100 reads on average across four biological replicates were analyzed. Genes with adjusted P-value <0.1 were considered to have significant expression change. **c.** Genes that exhibit up-regulated gene expression upon FTO depletion show longer gene length. The classifications of the genes correspond to **(b)**. P-values, Student's t-test. **d.** GSEA enrichment of the genes related to morphine addiction pathway (mmu05032). **e.** Shown are heatmaps demonstrating the genes in the core components in the morphine addiction pathway with significant differential expression (adjusted P-value < 0.1). **f.** A schematic diagram showing the impact on different components in the morphine addiction pathway upon FTO depletion. MOR, mu opioid receptor; KOR, kappa opioid receptor; GIRK, G-protein-gated inwardly rectifying K^+ channels; VGCC, voltage-gated Ca^{2+} channel; D1-MSN, D1 receptor–expressing medium spiny neuron; $GABA_A$, γ-Aminobutyric acid sub-type A receptor; VGAT, vesicular inhibitory amino acid transporter; VP, the ventral pallidum; SNr, the substantia Nigra pars reticulata.

GABA release by inhibiting adenylyl cyclase/cAMP/PKA signaling through Gαi/o and by regulating voltage-gated Ca^{2+} channels (VGCCs) and G-protein-gated inwardly rectifying K+ channels (GIRKs) through Gβγ, which disinhibits D1-MSNs and promotes reward[85,86]. FTO depletion reversed this gene expression signature at multiple nodes. It lowered Ca^{2+}/calmodulin-stimulated *Adcy1* and raised Ca^{2+}-inhibited *Adcy5* and PKA subunits (*Prkacb*, *Prkar2a*), which may lead to restoration of cAMP/PKA signaling that MOR normally controls[87]. It raised VGCC subunits (*Cacna1b*, *Cacna1c*, *Cacna1h*) and lowered GIRK subunits (*Kcnj3*, *Kcnj9*), which would neutralize the $G_{\beta\gamma}$-mediated effects of MOR on these channels[85]. It raised GABAA receptor subunits (*Gabrb1*, *Gabrb2*, *Gabrb3*, *Gabrd*, *Gabrg1*, *Gabrg3*) in D1-MSNs, which would strengthen the inhibitory currents that MOR activation reduces[84,88]. FTO-depletion led to increased expression of opioid receptor genes, most notably *Oprk1* (KOR), which would increase dynorphin/KOR anti-reward tone that counteracts MOR-driven reward[89-91], as well as *Oprm1* and *Oprd1*.

Together, these changes suggest a coordinated shift in the NAc shell transcriptome. Rather than acting on a single effector, FTO depletion alters many genes across the same circuit in directions that oppose MOR signaling, and this network-level shift may explain some of the reduction in morphine reward.

Discussion

Morphine and other mu opioids remain among the most effective analgesics in pain management, yet their clinical use is limited by tolerance, reward and addiction, the properties that drive the escalation underlying opioid use disorder. A long-standing goal has been to separate these harmful properties from analgesia, so that pain can be relieved without promoting

opioid misuse. Here we describe a mechanism that achieves this separation, in which elevated m^6Am in snRNA suppresses morphine reward and tolerance while preserving analgesia. We uncovered this mechanism using genetic depletion of FTO and pharmacological FTO inhibition, which both reduced morphine reward and antinociceptive tolerance without altering morphine analgesia. Because FTO is known mainly as a demethylase of m^6A in mRNA, we expected these effects would be associated with increased levels of m^6A on specific mRNAs. Instead, we found that FTO depletion leads to increases in m^6Am in snRNA, pointing to m^6Am as a novel regulator of morphine reward and tolerance. Overall, our work shows that raising m^6Am in snRNA reduces the reward and tolerance produced by opioids while sparing their analgesic action, and establishes the control of RNA modifications in snRNA, and thus of snRNA function, as a new approach to separating the therapeutic and harmful effects of opioids.

To find the RNA substrate of FTO, we mapped m^6A and m^6Am across the NAcSh transcriptome using direct RNA sequencing and CROWN-seq, respectively. These methods provide highly quantitative measurements of m^6A and m^6Am stoichiometry. Our analysis of 20,139 m^6A sites showed no clear increase in stoichiometry in any m^6A site in any mRNA after FTO depletion. FTO depletion instead led to marked increases in m6Am stoichiometry in snRNA. To test whether this rise in m^6Am was responsible for the behavioral effects, we used a genetic strategy, reasoning that if elevated m^6Am mediates the effects of FTO loss, then removing the m^6Am biosynthetic enzyme PCIF1 should mitigate the effects of FTO depletion. When we co-depleted *Fto* and *Pcif1*, FTO depletion no longer suppressed morphine reward and tolerance. This epistasis experiment supports the conclusion that elevated m^6Am mediates the beneficial effects of FTO depletion.

How could a modification on snRNA control morphine reward and tolerance? snRNAs are the core components of the spliceosome, where they direct the recognition and removal of introns, and U1 snRNA has a further role in promoting transcriptional elongation through introns and 3'UTRs[80]. A modification that alters snRNA function could therefore reshape gene expression broadly, through both splicing and elongation. Our data supports this idea. FTO depletion changed alternative splicing at thousands of sites across the transcriptome, with exon skipping as the predominant change, and it also shifted gene expression in a way that favored longer genes, consistent with an effect on U1-dependent elongation. These changes were not confined to a few transcripts but were spread across the transcriptome, and the resulting set of altered genes was enriched for components of the morphine addiction pathway. We therefore propose that elevated m^6Am in snRNA reduces morphine reward and tolerance by altering snRNA function, which remodels splicing and elongation across many genes and, through this broad change, shifts the expression of morphine-pathway genes.

An interesting feature of this mechanism is that it operates in two separate areas for the two behaviors. When we depleted *Fto* in NAcSh, morphine reward was reduced but tolerance was intact, whereas depletion in the DRG reduced tolerance but left reward unchanged. Reward and tolerance are therefore controlled by FTO at anatomically distinct sites, a central reward circuit for one and a peripheral sensory ganglion for the other, suggesting that the role of FTO in regulating the actions of mu opioids is region-specific.

Our transcriptomic and m^6A/m^6Am mapping studies were performed using bulk NAc tissue, which does not provide single-cell resolution. Future work using single cell-RNAseq or spatial transcriptomics will be necessary to define the molecular mechanisms driving these changes at the level of individual cells or neurons. Although this work focused on the NAcSh

and DRG, additional brain regions, such as the VTA, mPFC, and PAG, are also involved in opioid reward or tolerance. We plan to investigate the role of FTO in these regions in future studies.

These findings point to FTO as a therapeutic target for reducing the harmful effects of opioids. An FTO inhibitor given alongside an opioid could lessen the reward and tolerance while preserving pain relief. The reduction of fentanyl tolerance by the FTO inhibitor suggests that this benefit would extend across mu opioids rather than being specific to morphine. A therapy that inhibits FTO would also be expected to have an acceptable safety profile. Global loss of FTO early in development is poorly tolerated in mice[42,92], but deletion restricted to adult animals has minimal pathologic effects[93]. The manipulations used in this study were both adult-onset and confined to specific tissues. Small-molecule FTO inhibitors have been used in animal cancer studies without severe toxicity[43]. FTO inhibitors may therefore represent a new class of adjuncts to mu opioids in pain management and opioid use disorder treatment.

References

1 Crime, U. N. O. o. D. a. World Drug Report 2021. (https://www.unodc.org/res/wdr2021/field/WDR21_Booklet_3.pdf, 2021).

2 Seth, P., Scholl, L., Rudd, R. A. & Bacon, S. Overdose Deaths Involving Opioids, Cocaine, and Psychostimulants - United States, 2015-2016. *MMWR. Morbidity and mortality weekly report* **67**, 349–358 (2018). https://doi.org/10.15585/mmwr.mm6712a1

3 Volkow, N. D. The epidemic of fentanyl misuse and overdoses: challenges and strategies. *World Psychiatry* **20**, 195–196 (2021). https://doi.org/10.1002/wps.20846

4 Baumann, M. H., Kopajtic, T. A. & Madras, B. K. Pharmacological Research as a Key Component in Mitigating the Opioid Overdose Crisis. *Trends Pharmacol Sci* **39**, 995–998 (2018). https://doi.org/10.1016/j.tips.2018.09.006

5 Hyman, S. E., Malenka, R. C. & Nestler, E. J. Neural mechanisms of addiction: the role of reward-related learning and memory. *Annu.Rev Neurosci* **29**, 565–598 (2006). https://doi.org/10.1146/annurev.neuro.29.051605.113009 [doi]

6 Robison, A. J. & Nestler, E. J. Transcriptional and epigenetic mechanisms of addiction. *Nat Rev Neurosci* **12**, 623–637 (2011). https://doi.org/nrn3111 [pii];10.1038/nrn3111 [doi]

7 Maze, I. & Nestler, E. J. The epigenetic landscape of addiction. *Ann N Y Acad Sci* **1216**, 99–113 (2011). https://doi.org/10.1111/j.1749-6632.2010.05893.x [doi]

8 Kalivas, P. W. & Volkow, N. D. The neural basis of addiction: a pathology of motivation and choice. *Am J Psychiatry* **162**, 1403–1413 (2005).

9 Koob, G. F. & Volkow, N. D. Neurocircuitry of addiction. *Neuropsychopharmacol* **35**, 217–238 (2010). https://doi.org/npp2009110 [pii];10.1038/npp.2009.110 [doi]

10 Trujillo, K. A. & Akil, H. Inhibition of morphine tolerance and dependence by the NMDA receptor anagonist MK-801. *Science* **251**, 85–87 (1991).

11 Babey, A. M. *et al.* Nitric oxide and opioid tolerance. *Neuropharmacology* **33**, 1463–1470 (1994).

12 Kolesnikov, Y. A. *et al.* Functionally differentiating two neuronal nitric oxide synthase isoforms through antisense mapping: Evidence for opposing NO actions on morphine analgesia and tolerance. *Proceedings of the National Academy of Sciences of the United States of America* **94**, 8220–8225 (1997).

13 King, M., Su, W., Chang, A., Zuckerman, A. & Pasternak, G. W. Transport of opioids from the brain to the periphery by P-glycoprotein: peripheral actions of central drugs. *Nat.Neurosci.* **4**, 268–274 (2001).

14 Way, E. L., Loh, H. H. & Shen, F. Morphine tolerance, physical dependence, and synthesis of brain 5-hydroxytryptamine. *Science* **162**, 1290–1292 (1968). https://doi.org/10.1126/science.162.3859.1290

15 Cox, B. M. & Osman, O. H. The role of protein synthesis inhibition in the prevention of morphine tolerance. *Br J Pharmacol* **35**, P373–374 (1969).

16 Xu, J. *et al.* Alternatively spliced mu opioid receptor C termini impact the diverse actions of morphine. *The Journal of clinical investigation* **127**, 1561–1573 (2017). https://doi.org/10.1172/JCI88760

17 Gupta, A. *et al.* Increased abundance of opioid receptor heteromers after chronic morphine administration. *Sci Signal.* **3**, ra54 (2010). https://doi.org/3/131/ra54 [pii];10.1126/scisignal.2000807 [doi]

18 He, S. Q. *et al.* Facilitation of mu-opioid receptor activity by preventing delta-opioid receptor-mediated codegradation. *Neuron* **69**, 120–131 (2011). https://doi.org/S0896-6273(10)00986-4 [pii];10.1016/j.neuron.2010.12.001 [doi]

19 Granados-Soto, V., Kalcheva, I., Hua, X. Y., Newton, A. & Yaksh, T. L. Spinal PKC activity and expression: role in tolerance produced by continuous spinal morphine infusion. *Pain* **85**, 395–404 (2000).

20 Mayer, D. J., Mao, J. & Price, D. D. The development of morphine tolerance and dependence is associated with translocation of protein kinase C. *Pain* **61**, 365–374 (1995). https://doi.org/10.1016/0304-3959(95)00023-l

21 Bohn, L. M., Gainetdinov, R. R., Lin, F. T., Lefkowitz, R. J. & Caron, M. G. Mu-opioid receptor desensitization by beta-arrestin-2 determines morphine tolerance but not dependence. *Nature* **408**, 720–723 (2000).

22 Bohn, L. M., Lefkowitz, R. J. & Caron, M. G. Differential mechanisms of morphine antinociceptive tolerance revealed in (beta)arrestin-2 knock-out mice. *The Journal of neuroscience : the official journal of the Society for Neuroscience* **22**, 10494–10500 (2002).

23 Wang, Y. *et al.* Blockade of PDGFR-β activation eliminates morphine analgesic tolerance. *Nat Med* **18**, 385–387 (2012). https://doi.org/10.1038/nm.2633

24 von Zastrow, M. Regulation of opioid receptors by endocytic membrane traffic: mechanisms and translational implications. *Drug Alcohol Depend* **108**, 166–171 (2010). https://doi.org/10.1016/j.drugalcdep.2010.02.014

25 Jia, G. *et al.* N6-methyladenosine in nuclear RNA is a major substrate of the obesity-associated FTO. *Nat Chem Biol* **7**, 885–887 (2011). https://doi.org/10.1038/nchembio.687

26 Meyer, K. D. *et al.* Comprehensive analysis of mRNA methylation reveals enrichment in 3' UTRs and near stop codons. *Cell* **149**, 1635–1646 (2012). https://doi.org/10.1016/j.cell.2012.05.003

27 Mauer, J. *et al.* FTO controls reversible m(6)Am RNA methylation during snRNA biogenesis. *Nat Chem Biol* **15**, 340–347 (2019). https://doi.org/10.1038/s41589-019-0231-8

28 Mauer, J. *et al.* Reversible methylation of m(6)A(m) in the 5' cap controls mRNA stability. *Nature* **541**, 371–375 (2017). https://doi.org/10.1038/nature21022

29 McTaggart, J. S. *et al.* FTO is expressed in neurones throughout the brain and its expression is unaltered by fasting. *PloS one* **6**, e27968 (2011). https://doi.org/10.1371/journal.pone.0027968

30 Gerken, T. *et al.* The obesity-associated FTO gene encodes a 2-oxoglutarate-dependent nucleic acid demethylase. *Science* **318**, 1469–1472 (2007). https://doi.org/10.1126/science.1151710

31 Li, Y. *et al.* N(6)-Methyladenosine Demethylase FTO Contributes to Neuropathic Pain by Stabilizing G9a Expression in Primary Sensory Neurons. *Adv Sci (Weinh)* **7**, 1902402 (2020). https://doi.org/10.1002/advs.201902402

32 Meyer, K. D. & Jaffrey, S. R. The dynamic epitranscriptome: N6-methyladenosine and gene expression control. *Nat Rev Mol Cell Biol* **15**, 313–326 (2014). https://doi.org/10.1038/nrm3785

33 Wei, J. *et al.* FTO mediates LINE1 m(6)A demethylation and chromatin regulation in mESCs and mouse development. *Science* **376**, 968–973 (2022). https://doi.org/10.1126/science.abe9582

34 Meyer, K. D. & Jaffrey, S. R. Rethinking m(6)A Readers, Writers, and Erasers. *Annu Rev Cell Dev Biol* **33**, 319–342 (2017). https://doi.org/10.1146/annurev-cellbio-100616-060758

35 Zhao, X. *et al.* FTO-dependent demethylation of N6-methyladenosine regulates mRNA splicing and is required for adipogenesis. *Cell Res* **24**, 1403–1419 (2014). https://doi.org/10.1038/cr.2014.151

36 Ruud, J. *et al.* The Fat Mass and Obesity-Associated Protein (FTO) Regulates Locomotor Responses to Novelty via D2R Medium Spiny Neurons. *Cell reports* **27**, 3182–3198.e3189 (2019). https://doi.org/10.1016/j.celrep.2019.05.037

37 Engel, M. *et al.* The Role of m(6)A/m-RNA Methylation in Stress Response Regulation. *Neuron* **99**, 389–403.e389 (2018). https://doi.org/10.1016/j.neuron.2018.07.009

38 Zhang, N., Ding, C., Zuo, Y., Peng, Y. & Zuo, L. N6-methyladenosine and Neurological Diseases. *Mol Neurobiol* **59**, 1925–1937 (2022). https://doi.org/10.1007/s12035-022-02739-0

39 Lei, C. & Wang, Q. The Progression of N6-methyladenosine Study and Its Role in Neuropsychiatric Disorders. *Int J Mol Sci* **23** (2022). https://doi.org/10.3390/ijms23115922

40 Annapoorna, P. K. *et al.* FTO: An Emerging Molecular Player in Neuropsychiatric Diseases. *Neuroscience* **418**, 15–24 (2019). https://doi.org/10.1016/j.neuroscience.2019.08.021

41 Shi, H., Wei, J. & He, C. Where, When, and How: Context-Dependent Functions of RNA Methylation Writers, Readers, and Erasers. *Molecular cell* **74**, 640–650 (2019). https://doi.org/10.1016/j.molcel.2019.04.025

42 Gao, X. *et al.* The fat mass and obesity associated gene FTO functions in the brain to regulate postnatal growth in mice. *PloS one* **5**, e14005 (2010). https://doi.org/10.1371/journal.pone.0014005

43 Huang, Y. *et al.* Small-Molecule Targeting of Oncogenic FTO Demethylase in Acute Myeloid Leukemia. *Cancer Cell* **35**, 677–691.e610 (2019). https://doi.org/10.1016/j.ccell.2019.03.006

44 Pianka, S. T. *et al.* D-2-HG Inhibits IDH1mut Glioma Growth via FTO Inhibition and Resultant m6A Hypermethylation. *Cancer Res Commun* **4**, 876–894 (2024). https://doi.org/10.1158/2767-9764.CRC-23-0271

45 Scofield, M. D. *et al.* The Nucleus Accumbens: Mechanisms of Addiction across Drug Classes Reflect the Importance of Glutamate Homeostasis. *Pharmacological reviews* **68**, 816–871 (2016). https://doi.org/10.1124/pr.116.012484

46 Castro, D. C. & Bruchas, M. R. A Motivational and Neuropeptidergic Hub: Anatomical and Functional Diversity within the Nucleus Accumbens Shell. *Neuron* **102**, 529–552 (2019). https://doi.org/10.1016/j.neuron.2019.03.003

47 Volkow, N. D. & Morales, M. The Brain on Drugs: From Reward to Addiction. *Cell* **162**, 712–725 (2015). https://doi.org/10.1016/j.cell.2015.07.046

48 Comer, S. D. & Cahill, C. M. Fentanyl: Receptor pharmacology, abuse potential, and implications for treatment. *Neurosci Biobehav Rev* **106**, 49–57 (2019). https://doi.org/10.1016/j.neubiorev.2018.12.005

49 Corder, G. *et al.* Loss of μ opioid receptor signaling in nociceptors, but not microglia, abrogates morphine tolerance without disrupting analgesia. *Nat Med* **23**, 164–173 (2017). https://doi.org/10.1038/nm.4262

50 Muchhala, K. H., Jacob, J. C., Dewey, W. L. & Akbarali, H. I. Role of β-arrestin-2 in short- and long-term opioid tolerance in the dorsal root ganglia. *Eur J Pharmacol* **899**, 174007 (2021). https://doi.org/10.1016/j.ejphar.2021.174007

51 Bagley, E. E., Chieng, B. C., Christie, M. J. & Connor, M. Opioid tolerance in periaqueductal gray neurons isolated from mice chronically treated with morphine. *Br J Pharmacol* **146**, 68–76 (2005). https://doi.org/10.1038/sj.bjp.0706315

52 Lueptow, L. M., Fakira, A. K. & Bobeck, E. N. The Contribution of the Descending Pain Modulatory Pathway in Opioid Tolerance. *Front Neurosci* **12**, 886 (2018). https://doi.org/10.3389/fnins.2018.00886

53 Pasternak, G. W. & Pan, Y. X. Mu opioids and their receptors: evolution of a concept. *Pharmacological reviews* **65**, 1257–1317 (2013). https://doi.org/65/4/1257 [pii];10.1124/pr.112.007138 [doi]

54 Williams, J. T. *et al.* Regulation of mu-opioid receptors: desensitization, phosphorylation, internalization, and tolerance. *Pharmacological reviews* **65**, 223–254 (2013). https://doi.org/10.1124/pr.112.005942

55 Jin, D., Chen, H., Zhou, M. H., Chen, S. R. & Pan, H. L. mGluR5 from Primary Sensory Neurons Promotes Opioid-Induced Hyperalgesia and Tolerance by Interacting with and Potentiating Synaptic NMDA Receptors. *The Journal of neuroscience : the official journal of the Society for Neuroscience* **43**, 5593–5607 (2023). https://doi.org/10.1523/jneurosci.0601-23.2023

56 Puig, S. & Gutstein, H. B. Chronic Morphine Modulates PDGFR-β and PDGF-B Expression and Distribution in Dorsal Root Ganglia and Spinal Cord in Male Rats. *Neuroscience* **519**, 147–161 (2023). https://doi.org/10.1016/j.neuroscience.2023.03.025

57 Ohashi, Y. *et al.* Yokukansan Inhibits the Development of Morphine Tolerance by Regulating Presynaptic Proteins in DRG Neurons. *Front Pharmacol* **13**, 862539 (2022). https://doi.org/10.3389/fphar.2022.862539

58 Fisher, C. *et al.* Morphine Efficacy, Tolerance, and Hypersensitivity Are Altered After Modulation of SUR1 Subtype K(ATP) Channel Activity in Mice. *Front Neurosci* **13**, 1122 (2019). https://doi.org/10.3389/fnins.2019.01122

59 He, X. T. *et al.* Inhibition of Histone Deacetylases Attenuates Morphine Tolerance and Restores MOR Expression in the DRG of BCP Rats. *Front Pharmacol* **9**, 509 (2018). https://doi.org/10.3389/fphar.2018.00509

60 Li, H., Tao, R., Wang, J. & Xia, L. Upregulation of miR-375 level ameliorates morphine analgesic tolerance in mouse dorsal root ganglia by inhibiting the JAK2/STAT3 pathway. *J Pain Res* **10**, 1279–1287 (2017). https://doi.org/10.2147/jpr.S125264

61 Ma, W., Zheng, W. H., Powell, K., Jhamandas, K. & Quirion, R. Chronic morphine exposure increases the phosphorylation of MAP kinases and the transcription factor CREB in dorsal root ganglion neurons: an in vitro and in vivo study. *Eur J Neurosci* **14**, 1091–1104 (2001). https://doi.org/10.1046/j.0953-816x.2001.01731.x

62 Walwyn, W., Evans, C. J. & Hales, T. G. Beta-arrestin2 and c-Src regulate the constitutive activity and recycling of mu opioid receptors in dorsal root ganglion neurons. *The Journal of neuroscience : the official journal of the Society for Neuroscience* **27**, 5092–5104 (2007). https://doi.org/10.1523/jneurosci.1157-07.2007

63 Zhang, Y., Wang, K., Lin, M., Li, Q. & Hong, Y. Inhibition of morphine tolerance by MrgC receptor via modulation of interleukin-1β and matrix metalloproteinase 9 in dorsal root ganglia in rats. *Eur J Pharmacol* **815**, 10–17 (2017). https://doi.org/10.1016/j.ejphar.2017.10.011

64 Lau, J. *et al.* Temporal control of gene deletion in sensory ganglia using a tamoxifen-inducible Advillin-Cre-ERT2 recombinase mouse. *Mol Pain* **7**, 100 (2011). https://doi.org/10.1186/1744-8069-7-100

65 Gaspari, S. *et al.* Nucleus accumbens-specific interventions in RGS9-2 activity modulate responses to morphine. *Neuropsychopharmacol* **39**, 1968–1977 (2014). https://doi.org/10.1038/npp.2014.45

66 Zachariou, V. *et al.* An essential role for DeltaFosB in the nucleus accumbens in morphine action. *Nat Neurosci* **9**, 205–211 (2006). https://doi.org/10.1038/nn1636

67 Sun, H. *et al.* Morphine epigenomically regulates behavior through alterations in histone H3 lysine 9 dimethylation in the nucleus accumbens. *The Journal of neuroscience : the official journal of the Society for Neuroscience* **32**, 17454–17464 (2012). https://doi.org/10.1523/jneurosci.1357-12.2012

68 Varaschin, R. K., Wazlawik, E. & Morato, G. S. Systemic and intra-accumbens microinjections of naltrexone interfere with tolerance to ethanol in rats. *Psychopharmacology* **182**, 366–374 (2005). https://doi.org/10.1007/s00213-005-0095-3

69 Hewel, C. *et al.* Direct RNA sequencing enables improved transcriptome assessment and tracking of RNA modifications for medical applications. *BioRxiv* (2025). https://doi.org/10.1101/2024.07.25.605188

70 Cruciani, S. & Novoa, E. M. The new era of single-molecule RNA modification detection through nanopore base-calling models. *Nat Rev Mol Cell Biol* (2025). https://doi.org/10.1038/s41580-025-00896-3

71 Dorado. In: Nanoporetech. vol. 18 June 2024, v0.7.2 edn. https://github.com/nanoporetech/dorado/: Oxford Nanopore Technologies PLC.; 2024: Dorado is a high-performance, easy-to-use, open source basecaller for Oxford Nanopore.

72 Katopodi, X. L., Begik, O. & Novoa, E. M. Toward the use of nanopore RNA sequencing technologies in the clinic: challenges and opportunities. *Nucleic Acids Res* **53** (2025). https://doi.org/10.1093/nar/gkaf128

73 Pryszcz, L. P. *et al.* Rapid and accurate demultiplexing of direct RNA nanopore sequencing data with SeqTagger. *Genome research* **35**, 956–966 (2025). https://doi.org/10.1101/gr.279290.124

74 Liu, C. *et al.* Absolute quantification of single-base m(6)A methylation in the mammalian transcriptome using GLORI. *Nature biotechnology* **41**, 355–366 (2023). https://doi.org/10.1038/s41587-022-01487-9

75 Zou, Y. *et al.* A Comparative Evaluation of Computational Models for RNA modification detection using Nanopore sequencing with RNA004 Chemistry. *BioRxiv* (2025). https://doi.org/https://doi.org/10.1101/2025.02.03.636352

76 Xie, Y. Y. *et al.* Single-molecule direct RNA sequencing reveals the shaping of epitranscriptome across multiple species. *Nat Commun* **16**, 5119 (2025). https://doi.org/10.1038/s41467-025-60447-4

77 Su, R. *et al.* R-2HG Exhibits Anti-tumor Activity by Targeting FTO/m(6)A/MYC/CEBPA Signaling. *Cell* **172**, 90–105.e123 (2018). https://doi.org/10.1016/j.cell.2017.11.031

78 Liu, J. F., Hawley, B. R., Nicholson, L. S. & Jaffrey, S. R. Decoding m(6)Am by simultaneous transcription-start mapping and methylation quantification. *Elife* **13** (2025). https://doi.org/10.7554/eLife.104139
79 Wilkinson, M. E., Charenton, C. & Nagai, K. RNA Splicing by the Spliceosome. *Annu Rev Biochem* **89**, 359–388 (2020). https://doi.org/10.1146/annurev-biochem-091719-064225
80 Mimoso, C. A. & Adelman, K. U1 snRNP increases RNA Pol II elongation rate to enable synthesis of long genes. *Molecular cell* **83**, 1264–1279.e1210 (2023). https://doi.org/10.1016/j.molcel.2023.03.002
81 Di, C. *et al.* U1 snRNP Telescripting Roles in Transcription and Its Mechanism. *Cold Spring Harb Symp Quant Biol* **84**, 115–122 (2019). https://doi.org/10.1101/sqb.2019.84.040451
82 Shen, S. *et al.* rMATS: robust and flexible detection of differential alternative splicing from replicate RNA-Seq data. *Proceedings of the National Academy of Sciences of the United States of America* **111**, E5593–5601 (2014). https://doi.org/10.1073/pnas.1419161111
83 Stuber, G. D., Britt, J. P. & Bonci, A. Optogenetic modulation of neural circuits that underlie reward seeking. *Biol Psychiatry* **71**, 1061–1067 (2012). https://doi.org/10.1016/j.biopsych.2011.11.010
84 Koo, J. W. *et al.* Loss of BDNF signaling in D1R-expressing NAc neurons enhances morphine reward by reducing GABA inhibition. *Neuropsychopharmacol* **39**, 2646–2653 (2014). https://doi.org/10.1038/npp.2014.118
85 Reeves, K. C., Shah, N., Muñoz, B. & Atwood, B. K. Opioid Receptor-Mediated Regulation of Neurotransmission in the Brain. *Front Mol Neurosci* **15**, 919773 (2022). https://doi.org/10.3389/fnmol.2022.919773
86 Khan, F. & Mehan, A. Addressing opioid tolerance and opioid-induced hypersensitivity: Recent developments and future therapeutic strategies. *Pharmacol Res Perspect* **9**, e00789 (2021). https://doi.org/10.1002/prp2.789
87 Ostrom, K. F. *et al.* Physiological roles of mammalian transmembrane adenylyl cyclase isoforms. *Physiol Rev* **102**, 815–857 (2022). https://doi.org/10.1152/physrev.00013.2021
88 Ostroumov, A. & Dani, J. A. Inhibitory Plasticity of Mesocorticolimbic Circuits in Addiction and Mental Illness. *Trends Neurosci* **41**, 898–910 (2018). https://doi.org/10.1016/j.tins.2018.07.014
89 Funada, M., Suzuki, T., Narita, M., Misawa, M. & Nagase, H. Blockade of morphine reward through the activation of kappa-opioid receptors in mice. *Neuropharmacology* **32**, 1315–1323 (1993). https://doi.org/10.1016/0028-3908(93)90026-y
90 Narita, M. *et al.* Direct evidence for the involvement of the mesolimbic kappa-opioid system in the morphine-induced rewarding effect under an inflammatory pain-like state. *Neuropsychopharmacol* **30**, 111–118 (2005). https://doi.org/10.1038/sj.npp.1300527
91 Suzuki, T., Kishimoto, Y., Misawa, M., Nagase, H. & Takeda, F. Role of the kappa-opioid system in the attenuation of the morphine-induced place preference under

chronic pain. *Life Sci* **64**, Pl1–7 (1999). https://doi.org/10.1016/s0024-3205(98)00537-2

92 Hess, M. E. *et al.* The fat mass and obesity associated gene (Fto) regulates activity of the dopaminergic midbrain circuitry. *Nat Neurosci* **16**, 1042–1048 (2013). https://doi.org/10.1038/nn.3449

93 McMurray, F. *et al.* Adult onset global loss of the fto gene alters body composition and metabolism in the mouse. *PLoS Genet* **9**, e1003166 (2013). https://doi.org/10.1371/journal.pgen.1003166

Methods

Animals

C57BL/6J (B6) (stock#: 000664) and Advillin-Cre-ERT2 mouse (Stock #: 032027) were obtained from Jackson Laboratory. *Fto*$^{fl/fl}$ mice in B6 background were obtained from Dr. Pumin Zhang, Baylor College of Medicine. *Pcif1*$^{fl/fl}$ mice in B6 background were obtained from Dr. Eric Lieberman Greer, Washington University School of Medicine. We bred *Fto*$^{fl/fl}$ mice with *Pcif1*$^{fl/fl}$ mice to generate *Fto*$^{fl/fl}$;*Pcif1*$^{fl/fl}$ mice and bred *Fto*$^{fl/fl}$ mice with Advillin-Cre-ERT2 (AvCreERT2) mice to produce *Fto*$^{fl/fl}$;AvCreERT2 mice. *Fto*$^{fl/fl}$;*Pcif1*$^{fl/fl}$ mice were bred with AvCreERT2 mice to produce *Fto*$^{fl/fl}$;*Pcif1*$^{fl/fl}$;AvCreERT2 mice. Adult (9 – 16 weeks-old) male mice were used in all experiments. All mice were housed in groups of five, maintained on a 12-h light/dark cycle and given *ad libitum* access to food and water. All animal studies were approved by the Institutional Animal Care and Use Committee of Rutgers New Jersey medical School.

Drug administration

FB23-2 (Millipore Sigma) or DMSO (Vehicle control) was administered by i.c.v. (20 µg) or i.p. (20 mg/kg) once a day for 4 or 5 days followed by morphine (s.c.) injection two hours later.

Fto$^{fl/fl}$;AvCreERT2 or *Fto*$^{fl/fl}$;*Pcif1*$^{fl/fl}$;AvCreERT2 mice were administered with tamoxifen (75 mg/kg, i.p., once per day for consecutive 10 days) prepared in corn oil or with corn oil as vehicle control.

Opioid analgesia

Analgesia was determined 30 min after subcutaneous (s.c.) injection using a radiant-heat tail-flick assay or hot-plate assay, with a maximal latency of 10 sec or 30 sec, respectively, to minimize tissue damage, as previously described[94,95]. Results were calculated as the percentage of maximum possible effect (% MPE) [(latency after drug – baseline latency)/(10 – baseline latency)*100]. Morphine doses used in cumulative dose-response studies were 0.3, 1, 3, 10 or 30 mg/kg. ED_{50} values were determined using nonlinear regression analysis (GraphPad Prism 10).

Opioid tolerance

Morphine tolerance was induced by twice-daily injections with morphine (10 mg/kg, s.c.) for 5 days. Morphine analgesia was examined on Days 1 and 5 by dose-response curves. Fentanyl tolerance was induced by an s.c. implanted osmotic pump (Alzet Model: 1007D; 1 mg/kg/day/mouse for 7 days). Tolerance was assessed by cumulative dose-response curve (Morphine doses: 1, 3, 10 and 30 mg/kg; Fentanyl doses: 0.01, 0.04, 0.1 and 0.3 mg/kg) on Days 1 and 5 or 7 with radiant heat tail-flick assay, by which the ED_{50} values were determined, as well as analgesic time courses with a fixed dose on Days 3, 4, 5 or 6 (morphine, 10 mg/kg, s.c.; fentanyl, 0.12 mg/kg, s.c.).

Conditioned place preference (CPP)

CPP was performed using a three-chamber apparatus (Med Associates) with a 6-day paradigm. On day 1, mice were placed in the central chamber for 1 min of habituation with the sliding doors closed, followed by a 20 min preconditioning period of free exploration in the three chambers. Time spent in each chamber was recorded. On days 2 – 5, mice were intraperitoneally (i.p.) injected with saline (morning) or morphine (10 mg/kg, afternoon), and confined to either the black or the white chamber for 20 min. On day 6, mice were placed for a 1 min habituation in the central chamber and followed by a 20 min free exploration in the three chambers. Time spent in each chamber was recorded. Preference is defined as difference between the times spent in the morphine-paired side of the chamber on the test day (Day 6) as compared to the preconditioning day (Day 1).

Stereotaxic microinjection of AAV vectors

AAV5-CMV-GFP/Cre (AAV-Cre) and AAV5-CMV-GFP (AAV-GFP, Control) with >5.6 x 10^{12} titers were obtained from the Vector Core at the University of North Carolina. AAVs were bilaterally microinjected into the NAc shell (NAcSh, Coordinates (in mm): AP +1.6, DV -4.55, ML ±0.55.) using a robot stereotaxic system (Neurostar). Mice were recovered for 4-5 weeks after microinjection to allow sufficient Cre expression before behavioral tests.

RNAscope and immunohistochemistry (IHC)

Mice were anaesthetized with Ketamine/Xylazine and transcardially perfused with PBS followed by 4% paraformaldehyde. Brain and DRG were dissected, post-fixed overnight, incubated in a sucrose gradient (20-30%), embedded in OCT medium (Tissue-Tek) and cryosectioned with 10 μm sections. RNAscope was performed on sections using RNAscope Kit (ACD, Catalog #:

322360) with Fto probe (Advanced Cell Diagnostics (ACD), Catalog #: 434261) and/or Pcif1 probe (ACD, Catalog #: 157913), as well as Opal fluorophores (Akoya Biosciences), in ACD HybEZ™ II Hybridization System, following the manufactural protocol. The DRG sections were then used in IHC with an anti-NeuN antibody (Millipore Sigma) and a Goat anti-Chicken 2nd antibody conjugated with Alexa Flour 488 following RNAscope procedure. The sections were then imaged for Fto or Pcif1/GFP in brain sections and for Fto or Pcif1/NeuN with a Nikon Ti2 HCA inverted fluorescent microscope.

Statistics

All mice were randomized and assigned to groups. Some, but not all, experiments were performed under blind conditions. All statistical analysis was carried out using GraphPad Prism 10. A student *t*-test, 1-way ANOVA or 2-way ANOVA was performed with *post hoc* Bonferroni's multiple comparisons test as described in the figure legend. Data represented the means ± SEM. Statistical significance was set at $p < 0.05$.

Differential gene expression analysis via RNA-seq

RNA-seq were performed by NovoGene. The sequencing reads were first trimmed by Cutadapt to remove adapter sequences[96]. The trimmed reads were then mapped to reference genome (GRCm39, Ensembl r107) via HISAT2 (key parameters: --fr unstranded[97]. To count the number of reads mapped to each genes in the reference, HTSeq-count was used[98]. Differential expression was performed with DESeq2 based on the read counts[99]. Only protein coding genes with at least 100 reads on average across all samples were considered. To analyze the gene lengths, for each

gene, we selected the longest isoform (including all exons and introns) based on the Ensembl gene annotations.

Alternative splicing analysis

Alternative splicing analysis was performed with rMATS (v4.3)[82]. The BAM files mapped by HISAT2 were used. Key parameters: -t paired, --readLength 150, --library-type fr-unstranded --variable-read-length.

GSEA analysis

GSEA analyses were performed with gseGO (nPerm = 10000, minGSSize = 3, maxGSSize = 800, pvalueCutoff = 0.1, pAdjustMethod = "fdr") and gseKEGG (minGSSize = 10, maxGSSize = 800, pvalueCutoff = 0.1, pAdjustMethod = "fdr") from clusterProfiler[100].

Nanopore direct RNA library preparation and sequencing

RNA sequencing libraries were prepared from total RNA using the nanopore direct RNA sequencing kit (ONT, SQK-RNA004) according to the manufacturer's instructions, with some notable adjustments. Samples were multiplexed following the SeqTagger method from Pryszcz et al. 2025[73] using the custom RT adapters for the b96_RNA004 model. In brief, 500 ng total RNA was barcoded with custom RT adapters via ligation with T4 DNA ligase (NEB, M0202L); next, samples were reverse transcribed with Induro Reverse Transcriptase (NEB, M0681L), cleaned-up with 1.8X AMPureXP beads (Beckman, A63881), and pooled together. The remaining library preparation steps were followed according to ONT kit instructions. Samples were loaded onto a

PromethION flow cell (ONT, Flo-PRO0004RA) and sequenced on a PromethION for 48 hours, acquiring 6.19 Gigabases and 5.87 M reads with an N50 read length of 1.66 kb.

Nanopore data analysis

The raw POD5 sequencing data files were basecalled with Dorado v1.0.0 with the rna004_130bps_sup@5.2.0 m^6A_DRACH modification model. The POD5 files were also used to generate a demultiplexed pod5.demux.tsv.gz file following the SeqTagger protocol with model b96_RNA004[73]. Basecalled BAM files were mapped to the GRCm39 mouse genome using the Dorado aligner with the parameter --mm2-opts "-ax splice -k 14". Aligned reads were demultiplexed with the SeqTagger bam_split_by_barcode.py script, and then sorted and indexed with SAMtools v1.2.20. For increased read coverage, replicates were merged with SAMtools merge. Modification bed tables (mod.bed) were compiled using Modkit v0.2.8 with the pileup command and the parameter --filter-threshold 0.99.

CROWN-seq experiments

The manuscript of modified CROWN-seq is under submission at the time of submission of this study. Briefly, to study snRNA m^6Am stoichiometries, we used a modified protocol of CROWN-seq[78], in which 2'-*O*-methyladenosine (Am) is chemically converted into 2'*O*-methylinosine (Im) and *N*6,2'*O*-dimethyladenosine (m^6Am) remains unconverted, allowing for m^6Am quantification. To enrich snRNA, short RNAs (17-200 nt) were isolated from total RNA using RCC-5 (Zymo Research, Cat#: R1016), and 100 ng of the small RNA fraction was used as input. Samples were chemically converted following the GLORI v2.0[101] conversion conditions. After clean-up, 10 ng of Drosophila melanogaster embryo Poly A+ RNA (Takara Bio, Cat#: 636224)

was spiked-in for QC. For precise capture of capped RNA species, samples were sequentially dephosphorylated with Quick CIP (NEB, Cat#: M0525L), decapped with mRNA Decapping Enzyme (NEB, Cat#: M0608S), 5' ligated with a 5' adapter (rCrCrUrArCrArCrGrArCrGrCrUrCrUrUrCrCrGrArUrCrUrNrNrNrNrNrNrNrNrNrNrUrUrA) and T4 RNA ligase 1 (NEB, Cat#: M0437M), and end-repaired with T4 PNK (NEB, Cat#: M0201L). Library preparation was completed by 3' adapter incorporation and cDNA synthesis via a template switching reaction with Induro reverse transcriptase (NEB, Cat#: M0681L) and indexing PCR with Phusion High-Fidelity PCR Master Mix with HF Buffer (NEB, Cat#: M0531L) and NEBNext primers (NEB, Cat#: E7780S). The amplified libraries were purified and size selected sequentially with AMPureXP (Beckman Coulter, Cat#: A63881) and SPRIselect (Beckman Coulter, Cat#: B23317) beads to remove short amplicons without inserted sequences. Libraries were pooled and sequenced by NovaSeqX by Weill Cornell Genomics Resources Core Facility.

CROWN-seq analysis

Quantifying snRNA methylation in mice is challenging because there are many copies of the same snRNA sequence in the mouse genome. As a result, many reads originating from snRNA fail to uniquely map to a genomic locus via genomic mapping or a transcript isoform via transcriptomic mapping. To overcome this issue, we performed a snRNA-type-specific analysis. In this analysis, we focused on the type of snRNA the reads mapped to. To do so, we first mapped the reads to all possible snRNA sequences via Bowtie2. We then grouped the reads based on a customized dictionary which maps different snRNA isoforms to their type of snRNA.

After assigning the reads to a specific snRNA type, we calculate the non-conversion rates of the first nucleotides.

Data and Code availability

All sequencing data generated from this study can be accessed from NCBI Gene Expression Omnibus (GEO):

- GSE334880 for nanopore direct RNA sequencing data (reviewer token: mpozqeokxnihvqj);
- GSE334881 for CROWN-seq data (reviewer token: wdituecqvrmdlcp) ;
- GSE335428 for NovoGene RNA-seq data (reviewer token: epehwmeihpipnsn).

The CROWN-seq analysis pipeline is available on GitHub:

https://github.com/jhfoxliu/CROWN-seq-lite

94 Pan, Y. X. *et al.* Involvement of exon 11-associated variants of the mu opioid receptor MOR-1 in heroin, but not morphine, actions. *Proc.Natl.Acad.Sci.U.S.A* **106**, 4917–4922 (2009). https://doi.org/0811586106 [pii];10.1073/pnas.0811586106 [doi]

95 Xu, J. *et al.* Stabilization of morphine tolerance with long-term dosing: Association with selective upregulation of mu-opioid receptor splice variant mRNAs. *Proceedings of the National Academy of Sciences of the United States of America* **112**, 279–284 (2015). https://doi.org/1419183112 [pii];10.1073/pnas.1419183112 [doi]

96 Martin, M. Cutadapt removes adapter sequences from high-throughput sequencing reads. *EMBnet journal* **17**, 10–12 (2011). https://doi.org/https://doi.org/10.14806/ej.17.1.200

97 Kim, D., Paggi, J. M., Park, C., Bennett, C. & Salzberg, S. L. Graph-based genome alignment and genotyping with HISAT2 and HISAT-genotype. *Nature biotechnology* **37**, 907–915 (2019). https://doi.org/10.1038/s41587-019-0201-4

98 Anders, S., Pyl, P. T. & Huber, W. HTSeq--a Python framework to work with high-throughput sequencing data. *Bioinformatics* **31**, 166–169 (2015). https://doi.org/10.1093/bioinformatics/btu638

99 Love, M. I., Huber, W. & Anders, S. Moderated estimation of fold change and dispersion for RNA-seq data with DESeq2. *Genome biology* **15**, 550 (2014). https://doi.org/10.1186/s13059-014-0550-8

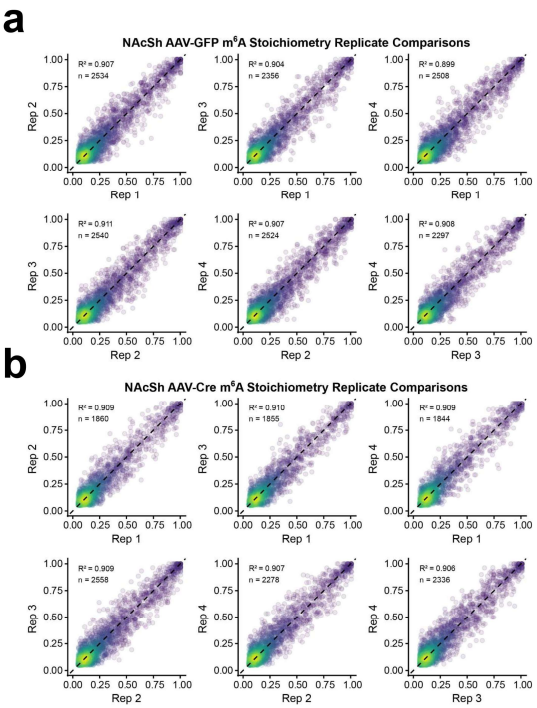
100 Yu, G., Wang, L. G., Han, Y. & He, Q. Y. clusterProfiler: an R package for comparing biological themes among gene clusters. *Omics* **16**, 284–287 (2012). https://doi.org/10.1089/omi.2011.0118

101 Sun, H. *et al.* Mild and ultrafast GLORI enables absolute quantification of m6A methylome from low-input samples. *Nature methods* **22**, 1226–1236 (2025). https://doi.org/10.1038/s41592-025-02680-9

Acknowledgements We thank Dr. Pumin Zhang at Baylor College of Medicine to provide *Fto*$^{fl/fl}$ mice. This work is supported by grants from the National Institutes of Health (R01DA09544 to Y.X.P., and S.R.J, DA060222 to Y.-X.P., R01DA037755 and RM1HG011563 to S.R.J., R01DK142785 to Y.-X.T., R01AI151215 to E.L.G., R01DA054368 and R01DA053261 to A.M.R., F31 DA060029 to A.F.M. and T32 DA055569 to R.C); and grants from the Department of Anesthesiology, New Jersey Medical School and Brain Health Institute, Rutgers.

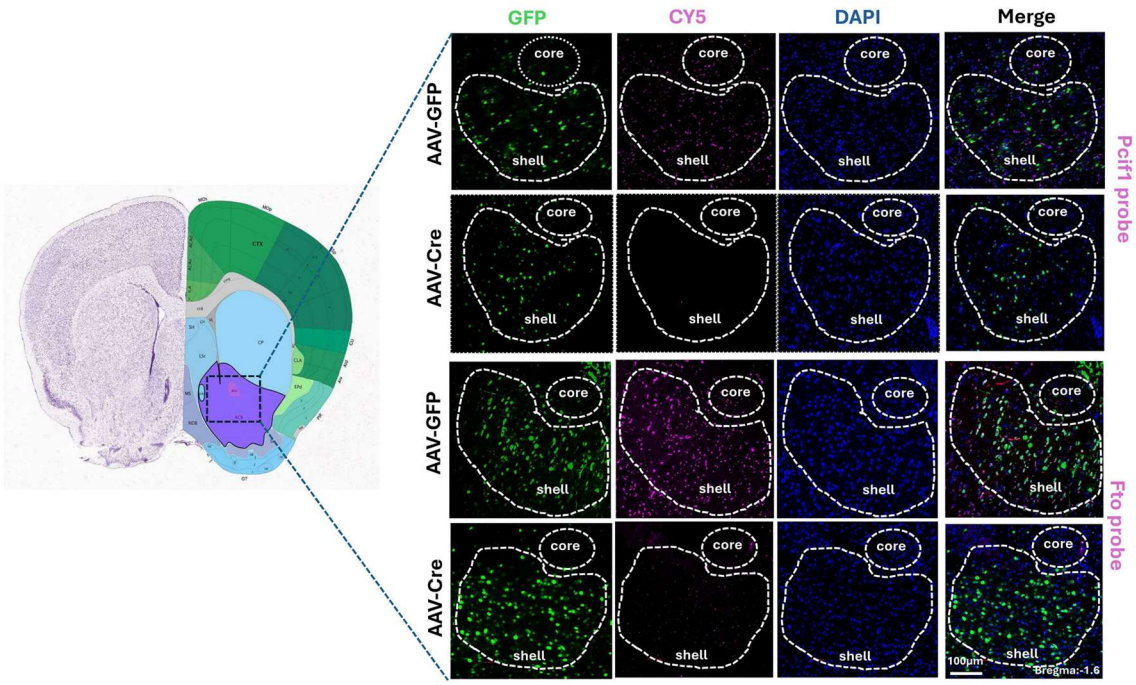
Author contributions Conceptualization, Y.-X.P., S.R.J., A.M.R., Y.-X.T. and E.L.G.; methodology, L.S., A.F.M., R.C., J.L., L.S.N., J.X., K.D., V.P., V.P.L., A.M.R., K.B. and B.W.; supervision, Y.-X.P., S.R.J., A.M.R., Y.-X.T. and E.L.G.; validation, L.S., A.F.M., R.C., J.L., L.S.N., J.X., K.D. and V.P.; investigation, L.S., A.F.M., R.C., J.L. and L.S.N.; writing, Y.-X.P., S.R.J., L.S., A.F.M., R.C., J.L. and L.S.N.

Competing interests S.R.J. is the co-founder and/or has equity in Chimerna Therapeutics, 858 Therapeutics, and Lucerna Technologies. Y.-X.P. is a scientific co-founder of Sparian Biosciences. Rutgers University has filed US Nonprovisional Patent Application 19/756,799, ‘‘Pharmaceutical formulations and methods” (inventor: Y.-X.P)

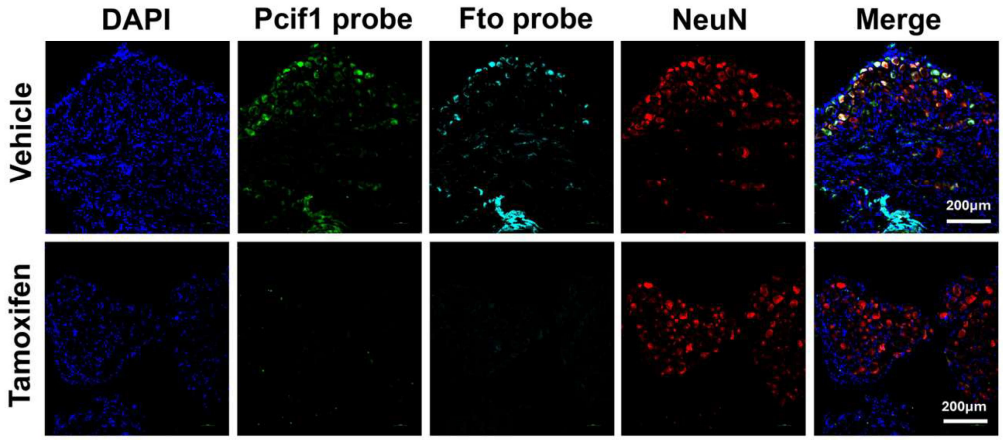


Extended Data Fig. 1. m^{6}A stoichiometry comparisons across biological replicates at each site

(A) and (**B**) Pairwise scatter plots comparing per-site m^{6}A stoichiometry calculations between four biological replicates (≥25 reads) of AAV-GFP treated (**A**) or AAV-Cre treated (**B**) *Fto*$^{fl/fl}$ mice. Pearson's coefficient of determination (R^2) and number of shared sites (n) are reported in each plot.

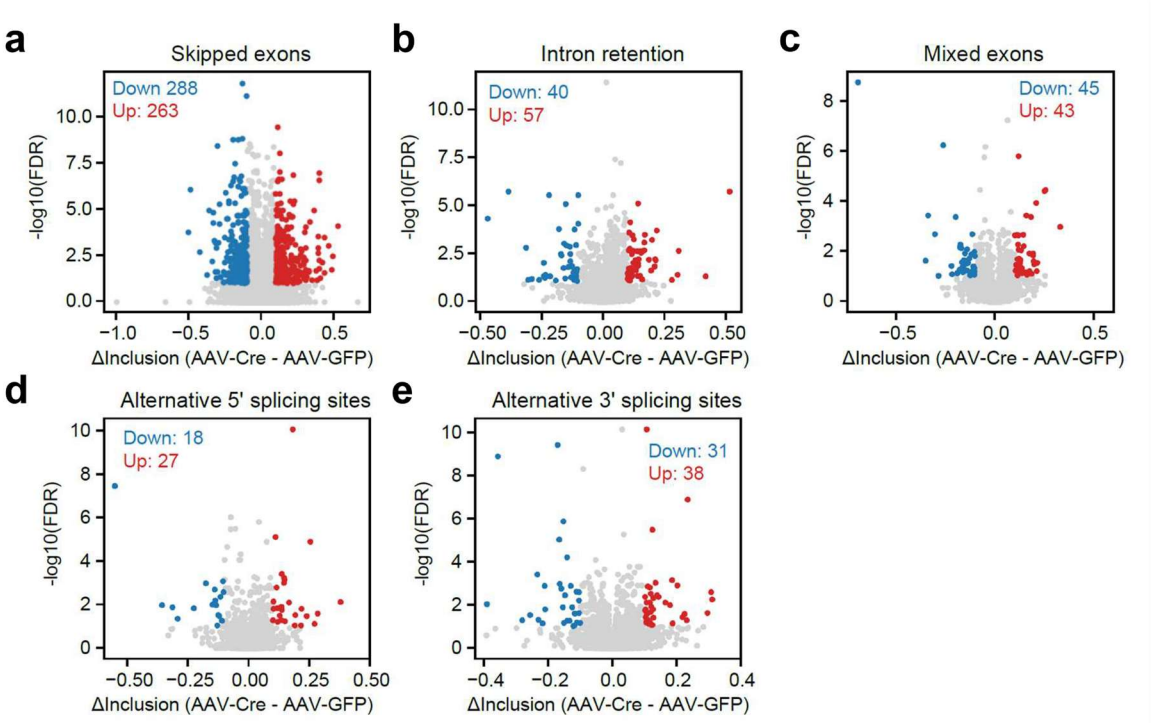


Extended Data Fig 2. Depletion of both Fto and Pcif1 in the NAcSh using microinjected AAV-Cre/GFP. RNAscope with Fto probe/Pcifi1 probe and Fto/Pcif1/GFP imaging was performed on brain sections from *Fto*$^{fl/fl}$;*Pcif1*$^{fl/fl}$ mice microinjected with AAV-Cre/GFP or AAV-GFP in the NAcSh after morphine CPP study, as described in the Methods. AAV-Cre: AAV5-CMV-Cre/GFP; AAV-GFP: AAV5-CMV-GFP; core: NAc core; shell: NAc shell (NAcSh).



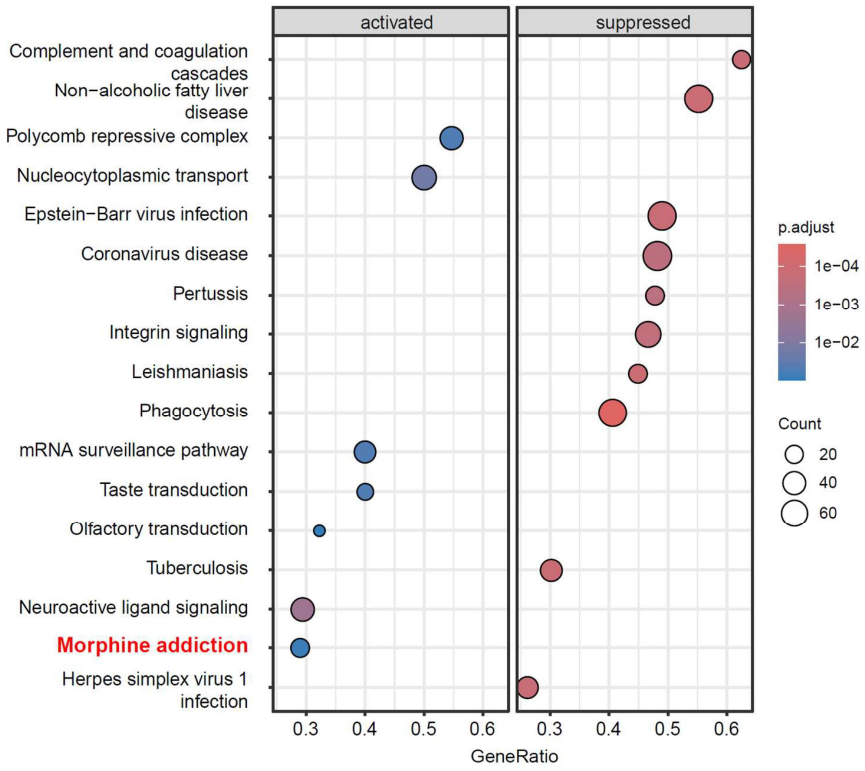
Extended Data Fig. 3. Depletion of both Fto and Pcif1 in the DRG sensory neurons using tamoxifen. Tamoxifen (75 mg/kg) or Corn oil (Vehicle) was i.p. administered daily in *Fto*$^{fl/fl}$;*Pcif1*$^{fl/fl}$;AvCreERT2 mice for 10 days. RNAScope combined with IHC with anti-NeuN antibody was performed on the DRG sections from perfused mice (4% PFA) after morphine tolerance study, as described in the Methods.

1109



Extended Data Fig. 4. Alternative splicing in mice NAcSh upon FTO depletion. (a) - (e), volcano plots showing the significant alternative splicing events (FDR < 0.1, |Δinclusion level| > 0.1) in different categories.

1110
1111
1112
1113



Extended Data Fig. 5. KEGG pathway analysis on mice NAcSh upon FTO depletion. Shown are top 17 KEGG pathways demonstrating significant enrichment in GSEA analysis. Pathways activated upon FTO depletion are shown on the left, while pathways suppressed upon FTO depletion are shown on the right.

Additional information

Supplementary Data Table 1. m^6A stoichiometry quantified by Nanopore sequencing

Supplementary Data Table 2. m^6Am stoichiometry quantified by CROWN-seq

Supplementary Data Table 3. Alternative splicing

Supplementary Data Table 4. Differential gene expression

Supplementary Data Table 5. GSEA analysis

Correspondence and requests for materials should be addressed to Samie Jaffrey or Ying-Xian Pan

Supplementary Files

This is a list of supplementary files associated with this preprint. Click to download.

- SupplementaryDataTable5.GSEA.xlsx
- SupplementaryDataTable4.Differentialexpression.xlsx
- SupplementaryDataTable2.m6Ammethylation.xlsx
- SupplementaryDataTable1.m6Amethylation.xlsx
- SupplementaryDataTable3.Alternativesplicing.xlsx